Astron. Astrophys. 324, 505–522 (1997)

ASTRONOMY
AND
ASTROPHYSICS

Core velocity dispersions for 25 Galactic and 10 old Magellanic globular clusters⋆ ,⋆⋆

Pierre Dubath[1,2], **Georges Meylan**[3], **and Michel Mayor**[1]

[1] Observatoire de Genève, ch. des Maillettes 51, CH-1290 Sauverny, Switzerland
[2] INTEGRAL Science Data Centre, ch. d'Écogia 16, CH-1290 Versoix, Switzerland
[3] European Southern Observatory, Karl-Schwarzschild-Str. 2, D-85748 Garching, Germany

Received 30 July 1996 / Accepted 13 September 1996

Abstract. We present, for 25 Galactic and 10 old Magellanic globular clusters, projected velocity dispersion (σ_p) measurements obtained by applying a cross-correlation technique to integrated-light spectra. In order to understand and estimate the statistical errors of these measurements due to small numbers of bright stars dominating the integrated light, we provide an extensive discussion based on detailed numerical simulations. These errors are smaller if the integration area is larger and/or the cluster concentration higher. The simulations show that measurements are reliable when the integrated light within the integration area is brighter than a given magnitude. The statistical errors on the σ_p measurements of Magellanic globular clusters are small because of a physically large integration area, whereas they can be important for measurements carried out over small central areas in Galactic clusters. The present observational results are used to outline a few characteristics of the globular cluster fundamental plane. In this respect, the old Magellanic globular clusters appear similar to the Galactic clusters.

Key words: (Galaxy:) globular clusters: general – stars: kinematics – techniques: radial velocities – galaxies: star clusters – Magellanic Clouds

1. Introduction

The fate of globular clusters is characterized by their dynamical evolution towards core collapse, a state of very high central stellar density. Most dynamical-evolution models predict that globular clusters may then experience a succession of expansion and contraction phases, the so-called gravothermal oscillations. The dynamical state of a cluster may be unveiled by the presence of cusps in both its surface-brightness and velocity-dispersion profiles. On the one hand, star counts from HST provide excellent insight into the innermost parts of a few high-concentration globular clusters, revealing, e.g., in the case of M15 (Guhathakurta et al. 1996, Sosin & King 1996, King et al. 1996) an unresolved core. On the other hand, spectroscopic observations of the same high-concentration clusters currently have lower spatial resolution.

At the center of globular clusters, radial velocities can be measured only for a limited number of individual stars because of the small number of bright stars, and also because of the crowding in the case of high-concentration clusters. Therefore, reliable velocity dispersions derived from radial velocities of individual stars can only be obtained over relatively large central areas: in general, larger than ten seconds of arc in radius. Over smaller areas, uncertainties due to small number statistic become important. An alternative is to obtain integrated-light spectra over small central apertures and to derive the velocity dispersion by measuring the Doppler line broadening due to the random spatial motions of the stars along the line of sight. However, even in this case, statistical uncertainty is a limitation because the contributions from a small number of bright stars can dominate the integrated light over small central areas. These observational difficulties are clearly illustrated in the case of M15 (see Peterson et al. 1989, and Dubath & Meylan 1994). Even by combining integrated-light measurements and radial velocities of individual stars, the statistical uncertainties are too large to allow the observations to constrain the shape of the velocity-dispersion profile in the inner few seconds of arc, i.e., in the area where the luminosity cusp is observed.

In contrast with the relatively large number of clusters for which radial-velocities are available from the literature, integrated-light measurements have only been carried out for a handful of Galactic and Magellanic globular clusters (e.g. Dubath et al. 1990, Mateo et al. 1991, Zaggia et al. 1992). In many Galactic high-concentration clusters, however, the integrated-light approach provides reliable velocity dispersions over small

Send offprint requests to: Pierre.Dubath@obs.unige.ch

⋆ Based on observations collected at the European Southern Observatory, La Silla, Chile

⋆⋆ Tables 6 and 7 are also available electronically at the CDS via anonymous ftp 130.79.1285 or
via http://cdsweb.v.strasbg.fr/Abstract.html

central areas, where crowding prevents the radial-velocity measurements of a large enough number of individual stars.

In the case of the Magellanic clusters, HST images show how difficult are the measurements of radial velocity of individual stars. Most of the time, several stars overlap on a typical seeing disk of $1''$, and the measurement of a bright star velocity can be biased by one, or several, close companions. For these clusters, the integrated-light measurements are carried out over areas physically larger, for practical reasons, than those used for Galactic clusters. These measurements therefore provide velocity dispersions averaged over larger areas, which are much less affected by statistical uncertainties, since the number of bright stars within those areas is large. For the above two reasons, the integrated-light approach can provide better results for any remote globular cluster, such as Magellanic clusters.

In this paper, we present integrated-light measurements of the velocity dispersions of relatively large numbers of high-concentration Galactic globular clusters, and of old Magellanic globular clusters. The uncertainties on these measurements due to small number statistic is carefully established by means of detailed numerical simulations. We give here some details on the data reduction and analysis techniques, as well as on the analysis of standard star results, which were not published in previous papers based on the same observational approach.

This new set of data is complementary to the radial velocity measurements, and often provides, for the Galactic clusters, the innermost data point of the velocity dispersion profile. These kinematical data are used to constrain and discriminate King-Michie (e.g., Meylan et al. 1995) and Fokker-Plank (e.g., Grabhorn et al. 1992) dynamical models. For example, our Galactic cluster data set is used in Pryor and Meylan (1993) to derive cluster masses and mass-to-light ratios.

This paper is structured as follows: Sect. 2 presents our observations, Sect. 3 describes our data reduction procedure, Sect. 4 provides precise results from the standard star measurements, Sect. 5 presents the results about the cluster radial velocities and core velocity dispersions, Sect. 6 presents a careful discussion of our estimates of the statistical errors on the σ_p measurements due to the small samples of stars contributing most of the luminosity, Sect. 7 compares our results with previous V_r measurements, Sect. 8 compares our results with previous σ_p measurements, Sect. 9 elaborates on the fundamental plane of the observed globular clusters, i.e., on the relation between the velocity dispersion, the luminosity, and a physical scale. Sect. 10 discusses the present results and summarizes this paper.

2. Observations

Integrated-light spectra of the core of 25 Galactic and 10 old Magellanic globular clusters were obtained with CASPEC, the Cassegrain echelle spectrograph of the European Southern Observatory (ESO) mounted on the ESO 3.6-m telescope at La Silla, Chile. A standard setup was used, with the 31.6 line mm^{-1} echelle grating. We performed the observations of the Galactic globular clusters during an observing run on July 6–8, 1989, and the observations of the Magellanic globular clusters during two observing runs on December 21–27, 1990 and on January 26, 1991. During each night, many standard stars were also observed. Spectra of thorium-argon lamps were taken before and after each exposure, with the telescope pointing towards the cluster or the standard star observed.

During each exposure on a cluster core, the entrance slit was scanned over the nucleus of the cluster in order to cover an area of $6'' \times 6''$ for the Galactic globular clusters and $5'' \times 5''$ for the Magellanic clusters. Such relatively large areas of integration allow us to reduce the statistical errors due to the domination of the integrated light by the contribution of a small number of bright stars at the center of some globular clusters (see Sect. 6 below). Table 1 gives the journal of our observations.

Table 1 displays, for each globular cluster observation, in column (1) the number allocated to this observation, in column (2) the NGC number of the cluster, in column (3) the date of the observation, in column (4) the dimension of the entrance slit, in column (5) the dimension of the integration (scanned) area, in column (6) the exposure time, in column (7) the CCD used for the observation, in column (8) the wavelength range, and in column (9) the spectral resolution. The spectral resolution is estimated from the typical full-width at half-maximum (FWHM) of the emission lines of the thorium-argon comparison spectra taken just before, or after, the cluster spectrum.

The charge coupled devices (CCDs) used are the # 8 and # 16 ESO CCDs. The ESO CCD # 8 is an RCA SID 503 high-resolution, thinned, backside-illuminated device, with 1024×640 pixels of $15 \times 15\,\mu$m^2 in size, and with a readout noise of about 24 electrons. The ESO CCD # 16 is a Tektronix TEK 512M-12, thinned, backside-illuminated device, with 512×512 pixels of $27 \times 27\,\mu$m^2 in size, and with a readout noise of about 10 electrons.

Observations with numbers 1, 2, 38, and 39 have been already described and exploited in previous papers (see Dubath et al. 1990 for observations # 38 and # 39, and Meylan et al. 1991 for observations # 1 and # 2).

3. Data reduction

The spectroscopic reduction is achieved with the ECHELLE package available in MIDAS, the ESO Munich Image Data Analysis System, following standard procedures. No flat-field operation is applied, since flux calibration is unnecessary when cross-correlating spectra for obtaining radial velocity or velocity dispersion values.

The reduced spectra are then cross-correlated with a numerical mask over their full spectral range. The properties of this mask, as well as the details of our cross-correlation technique, are described in a previous study concerning the Large Magellanic Clouds globular cluster NGC 1835 (Dubath et al. 1990). The numerical version of the physical mask used so far for optical cross-correlation in the spectrophotometer CORAVEL (COrrelation – RAdial – VELocities, see Baranne et al. 1979) is simply extended in order to encompass the spectral domains of all CASPEC spectrum orders (4200–6000 Å). This extension is computed following the procedure described in Baranne et al.

Table 1. Journal of the CASPEC integrated-light observations.

Obs # (1)	NGC # (2)	Observation Date (3)	Slit Size (arcsec^2) (4)	Scan Area (arcsec^2) (5)	Exp Time (min) (6)	CCD (7)	Wavelength Range (Å) (8)	Resolution (km s^{-1}) (9)
Galactic globular clusters								
1	104	1989 Jul 6	1.4 × 6	6 × 6	15	RCA_{HR}	4250–5270	13-14
2	"	1989 Jul 8	1.2 × 6	6 × 6	15	RCA_{HR}	4250–5270	13-14
3	362	1989 Jul 8	1.2 × 6	6 × 6	15	RCA_{HR}	4250–5270	13-14
4	1851	1991 Jan 26	2.1 × 5	5 × 5	20	TEK	4440–6000	17-18
5	1904	1991 Jan 26	2.1 × 5	5 × 5	20	TEK	4440–6000	17-18
6	5272	1989 Jul 8	1.2 × 6	6 × 6	30	RCA_{HR}	4250–5270	13-14
7	5286	1989 Jul 6	1.4 × 6	6 × 6	30	RCA_{HR}	4250–5270	13-14
8	5694	1989 Jul 8	1.2 × 6	6 × 6	60	RCA_{HR}	4250–5270	13-14
9	5824	1989 Jul 7	1.4 × 6	6 × 6	30	RCA_{HR}	4250–5270	13-14
10	5904	1989 Jul 7	1.4 × 6	6 × 6	40	RCA_{HR}	4250–5270	13-14
11	5946	1989 Jul 6	1.4 × 6	6 × 6	30	RCA_{HR}	4250–5270	13-14
12	6093	1989 Jul 8	1.2 × 6	6 × 6	30	RCA_{HR}	4250–5270	13-14
13	6256	1989 Jul 7	1.4 × 6	6 × 6	30	RCA_{HR}	4250–5270	13-14
14	6266	1989 Jul 6	1.4 × 6	6 × 6	30	RCA_{HR}	4250–5270	13-14
15	6284	1989 Jul 8	1.2 × 6	6 × 6	30	RCA_{HR}	4250–5270	13-14
16	6293	1989 Jul 6	1.4 × 6	6 × 6	30	RCA_{HR}	4250–5270	13-14
17	6325	1989 Jul 7	1.4 × 6	6 × 6	60	RCA_{HR}	4250–5270	13-14
18	6342	1989 Jul 8	1.2 × 6	6 × 6	60	RCA_{HR}	4250–5270	13-14
19	6397	1989 Jul 6	1.4 × 6	6 × 6	30	RCA_{HR}	4250–5270	13-14
20	"	1989 Jul 6	1.4 × 6	no scan	30	RCA_{HR}	4250–5270	13-14
21	6441	1989 Jul 8	1.2 × 6	6 × 6	30	RCA_{HR}	4250–5270	13-14
22	6522	1989 Jul 7	1.4 × 6	6 × 6	20	RCA_{HR}	4250–5270	13-14
23	6558	1989 Jul 7	1.4 × 6	6 × 6	60	RCA_{HR}	4250–5270	13-14
24	6681	1989 Jul 8	1.2 × 6	6 × 6	20	RCA_{HR}	4250–5270	13-14
25	6752	1989 Jul 6	1.4 × 6	6 × 6	30	RCA_{HR}	4250–5270	13-14
26	7078	1989 Jul 8	1.2 × 6	6 × 6	60	RCA_{HR}	4250–5270	13-14
27	7099	1989 Jul 7	1.4 × 6	6 × 6	30	RCA_{HR}	4250–5270	13-14
28	"	1989 Jul 7	1.4 × 6	6 × 6	30	RCA_{HR}	4250–5270	13-14
29	"	1989 Jul 7	1.4 × 6	6 × 6 S	60	RCA_{HR}	4250–5270	13-14
30	"	1989 Jul 7	1.4 × 6	6 × 6 W	60	RCA_{HR}	4250–5270	13-14
31	"	1989 Jul 8	1.2 × 6	6 × 6	30	RCA_{HR}	4250–5270	13-14
SMC globular clusters								
32	121	1989 Jul 6	6 × 6	1.4 × 6	30	RCA_{HR}	4250–5270	13-14
33	"	1989 Jul 6	6 × 6	1.4 × 6	60	RCA_{HR}	4250–5270	13-14
34	419	1990 Dec 24	2.1 × 5	5 × 5	20	TEK	4380–5880	17-18
LMC globular clusters								
35	1466	1990 Dec 21	2.1 × 5	5 × 5	30	TEK	4380–5880	17-18
36	1754	1990 Dec 21	2.1 × 5	5 × 5	40	TEK	4380–5880	17-18
37	1786	1990 Dec 22	2.1 × 5	5 × 5	10	TEK	4380–5880	17-18
38	1835	1987 Nov 11	1.2 × 6	6 × 6	30	RCA	4400–4500	14-15
39	"	1987 Nov 11	1.2 × 6	6 × 6	30	RCA	4400–4500	14-15
40	"	1990 Dec 25	2.1 × 5	5 × 5	15	TEK	4380–5880	17-18
41	1916	1990 Dec 21	2.1 × 5	no scan	15	TEK	4380–5880	17-18
42	"	1990 Dec 21	2.1 × 5	5 × 5	10	TEK	4380–5880	17-18
43	2005	1990 Dec 23	2.1 × 5	5 × 5	20	TEK	4380–5880	17-18
44	2019	1990 Dec 24	2.1 × 5	5 × 5	20	TEK	4380–5880	17-18
45	2210	1990 Dec 21	2.1 × 5	5 × 5	30	TEK	4380–5880	17-18
46	Ho 11	1991 Jan 26	2.1 × 5	5 × 5	30	TEK	4440–6000	17-18

Observations with numbers 1, 2, 38, and 39 have been already described and exploited in previous papers (see Dubath et al. 1990, and Meylan et al. 1991).

(1979), first, from the observed spectrum of Arcturus (Griffin 1968) – already used to build the original CORAVEL mask – in the wavelength range 4200–5500 Å, and second, from theoretical spectra in the wavelength range 5500–6000 Å (Bell & Gustafson 1993 private communication).

Our cross-correlation technique produces a cross-correlation function (CCF) – relative intensity as a function of radial velocity – which is nearly a perfect Gaussian (see Fig. 6 below). A Gaussian function

$$g(v) = 1 - D \exp(-(v - V_r)^2/2\sigma^2_{CCF}) \quad (1)$$

is fitted to each deduced CCF in order to determine three physical quantities: (1) the abscissa of its minimum, equal to the radial velocity V_r, (2) its depth D, related to the metallicity, and

(3) its standard deviation $\sigma_{\rm CCF}$, related to line broadening mechanisms. Comparison of the CCF of a globular cluster spectrum with the CCFs of standard star spectra unveils the broadening of the cluster CCF produced by the Doppler line broadening present in the integrated-light spectra because of the random spatial motions of the stars along the line of sight. When a large enough number of stars contributes significantly to the integrated light, i.e., when statistical errors are small, the CCF of an integrated-light spectrum of a globular cluster is the convolution of the CCF of the spectrum of a typical individual globular cluster star with the projected velocity distribution. A precise estimate of the projected stellar velocity dispersion σ_p in the integration area of the considered globular cluster is then given by the following quadratic difference,

$$\sigma_p^2 = \sigma_{\rm CCF}^2({\rm cluster}) - \sigma_{\rm ref}^2 \ , \qquad (2)$$

which is the difference between $\sigma_{\rm CCF}$, from the Gaussian fitted to the cluster CCF, and $\sigma_{\rm ref}$, the average of the $\sigma_{\rm CCF}$ obtained for a sample of standard stars as representative as possible of the cluster stars which contribute most of the integrated light. Equation (2) is valid only if the distribution of stellar radial velocities in the globular cluster is sufficiently close to a Gaussian distribution. This is confirmed (i) by the nearly perfect Gaussian shape of some of our globular cluster CCFs (Fig. 6 below), and (ii) by some recent studies based on relatively large number of radial velocities of individual stars, which show that the distribution of projected velocities is consistent with a Gaussian distribution (e.g., Reijns et al. 1993 and Meylan et al. 1995).

For each astronomical target, two independent wavelength calibrations are carried out, using the thorium-argon spectra taken before and after the target exposure. The two corresponding spectra are both used in the cross-correlation analysis. Their CCFs never differ significantly, either in terms of radial velocity V_r or in terms of standard deviation $\sigma_{\rm CCF}$. For a given spectrum, the final results of both quantities (V_r and $\sigma_{\rm CCF}$) are the average of the two determinations.

4. Results from the standard star measurements

The set of standard stars, observed during all observing runs, comprises (i) some IAU radial velocity standards along with some Southern faint CORAVEL radial velocity standards (Mayor & Maurice 1985), (ii) some nearby K-dwarf CORAVEL radial velocity standards, (iii) some giant stars members of three open clusters (NGC 2447 and NGC 2682 having solar metallicities, and NGC 2506 which is metal-deficient), and (iv) some metal-deficient red giants of the Galactic halo (Norris et al. 1985). Each of these standard stars has an accurate reference radial velocity (to better than 0.3 km s^{-1}) given by the average of numerous previous CORAVEL measurements. These measurements also show that none of these stars is variable in radial velocity.

All spectra of standard stars used in this study have relatively high S/N ratios ($\sim$ 30–50). Consequently, the influence of the spectrum noise – photon counting and CCD readout noises – on the measurements of radial velocities V_r and standard deviations $\sigma_{\rm CCF}$ from CCFs is completely negligible. Estimates of instrumental errors on both V_r and $\sigma_{\rm CCF}$ measurements are given from repeated measurements of the same star.

Table 2. Radial velocities of all standard stars measured in July 1989.

HD	$V_r^{\rm COR}$ (km s^{-1})	Jul 6 $V_r^{\rm CAS} - V_r^{\rm COR}$ (km s^{-1})	Jul 7 $V_r^{\rm CAS} - V_r^{\rm COR}$ (km s^{-1})	Jul 8 $V_r^{\rm CAS} - V_r^{\rm COR}$ (km s^{-1})	$\overline{V}_r^{\rm CAS}$ (km s^{-1})
(1)	(2)	(3)	(4)	(5)	(6)
IAU radial velocity standards					
107328	35.9±0.2	...	4.7	1.5	39.0
126053	−19.5±0.2	0.2	1.4	−1.5	−19.5±1.5
136202	54.2±0.2	0.6	...	...	54.8
145001	−10.7±0.3	...	2.4	...	−8.3
171391	7.1±0.2	0.2	1.0	−0.8	7.2±0.9
182572	−100.3±0.2	...	...	0.8	−99.5
187691	−0.2±0.2	−0.5	1.0	−0.1	−0.1±0.8
203638	21.7±0.2	0.5	1.1	0.6	22.4±0.3
223311	−20.7±0.2	0.6	...	...	−20.1
223647	14.9±0.2	...	−1.0	...	13.9
Faint southern CORAVEL radial velocity standards					
111417	−19.6±0.2	−1.1	−3.3	−1.2	−21.5±1.2
193231	−31.1±0.3	...	...	−1.9	−33.0
196983	−9.6±0.2	...	...	−0.3	−9.9
219509	67.3±0.2	...	−1.9	−2.1	65.3
Mean		0.1	0.6	−0.5	...
σ_{n-1}		0.6	2.4	1.2	...

4.1. *Zero-point offset and instrumental uncertainty of the radial velocity measurements*

All radial velocity measurements from all standard star spectra obtained during our three observing runs are presented in Tables 2 and 3, together with the CORAVEL reference radial velocities. The CORAVEL V_r are the average of many CORAVEL V_r measurements and are, in all cases, more accurate than the present measurements. Note that zero-point offset corrections have been applied to all of our V_r values ($V_r^{\rm CAS}$) given in this paper as explained below.

For each observing night, we compute the radial velocity zero-point offset of our measurements by comparing, for all of the standard stars observed, our V_r with the CORAVEL reference V_r. No significant variation in zero-point from night to night are observed in the first observing run, and a zero-point correction of -1.4 km s^{-1} is applied to all of our V_r measurements in order to have a radial velocity zero-point consistent with the CORAVEL one. For the second and third observing runs, we find that the zero-point offset of the measurements of the first night may be different from the zero-point offset of the measurements of the other 6 nights. We apply radial velocity corrections of -1.1 and -2.8 km s^{-1} to all measurements of the first and the other 6 nights, respectively, in order to have again zero-points consistent with the CORAVEL one.

It may be worth mentioning that the origin of these zero-point offsets is not understood. It may result from instrumental

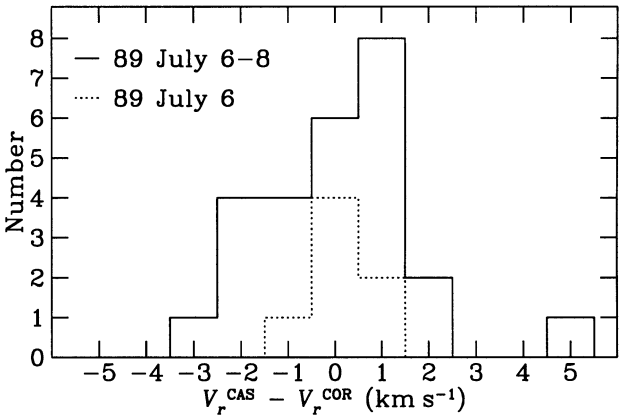

Fig. 1. Histogram of the differences between the present and the CORAVEL radial velocities for the standard stars measured in July 1989 (first observing run).

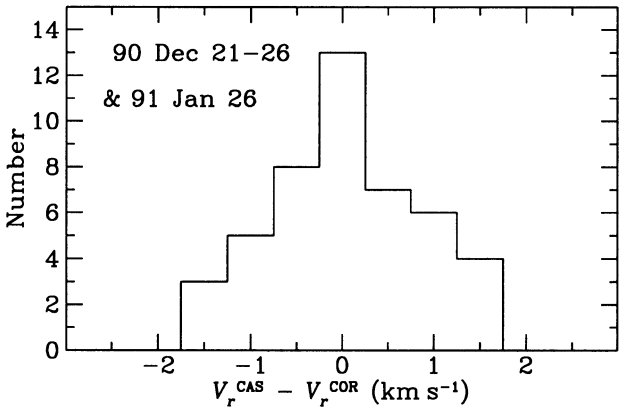

Fig. 2. Histogram of the differences between the present and the CORAVEL radial velocities for the standard star measured in December 1990 and January 1991 (second observing run).

problems. It is surprising to find variations from night to night. We seem to observe a significant difference between the first and the other six nights of the second and third runs.

Table 2 displays, for each standard star observed during the first observing run, in column (1) the HD number of the observed star, in column (2) the mean CORAVEL V_r with its uncertainty, in columns (3) to (5), for each night, the difference between the corrected present measurements and the CORAVEL V_r measurements, and in column (6) the mean corrected V_r of our measurements, with its standard deviation if the star is measured more than twice. The last two lines of this table give, for each night, the mean and the standard deviation of the differences between the present and the CORAVEL V_r measurements.

Table 3 displays, for each standard star observed during the second and third observing runs, in column (1) the identification number of the star observed, in column (2) the mean CORAVEL V_r and its uncertainty, in columns (3) to (9), for each night, the differences between the corrected present measurements and the CORAVEL V_r measurements, and in column (10) the mean corrected V_r of our measurements with its standard deviation, if the star is measured more than twice. The last two lines of this table give, for each night, the mean and the standard deviation of the differences between the present and the CORAVEL V_r measurements.

The quadratic mean standard deviations (internal error) of repeated measurements of the same star is 0.9 and 0.6 km s^{-1} for the first and second observing runs, respectively. The standard deviations of the differences between the present and CORAVEL V_r measurements are 1.6 and 0.8 km s^{-1} for the first and second observing runs, respectively. These second numbers provide external estimates of the present V_r measurement accuracy.

Figs. 1 and 2 present, for the first and second observing runs, respectively, the histograms of the differences between the present and the CORAVEL radial velocities. Fig. 3 displays these radial velocity differences as a function of the CORAVEL V_r, for all observing run measurements. Fig. 3 shows that no systematic radial velocity differences between the present and the CORAVEL V_r are observed as a function of the radial velocity.

It is worth mentioning that the radial velocity accuracy of 0.8 km s^{-1} obtained during the second observing run corresponds to roughly one twentieth of a spectral resolution element, i.e., to a shift on the CCD of about 1–2 tenths of a pixel along the dispersion direction. As the slit width corresponds roughly to one spectral resolution element on the CCD, an accuracy of ~ 1 km s^{-1} in radial velocity implies that, during the observation, the center of gravity of the star light is centered on the slit with an accuracy of about half a tenth of the slit width. Since the star centering on the slit is achieved by eye, such an accuracy is remarkable.

4.2. Intrinsic standard deviation $\sigma_{\rm ref}$ of stellar CCFs

The typical standard deviation $\sigma_{\rm ref}$ of the CCFs of stellar spectra is taken as the mean of the $\sigma_{\rm CCF}$ measurements obtained for the subsample of standard giant stars of spectral types in the range G5–K5. These stars are chosen because they are representative of the red and asymptotic giant-branch stars, which contribute most to the integrated light of a globular cluster.

4.2.1. $\sigma_{\rm ref}$ from July 1989

For each standard star observed in July 1989, Table 4 displays in column (1) its HD number, in column (2) its spectral type, in columns (3) to (5) the $\sigma_{\rm CCF}$ measurements obtained during the different nights, and in column (6) the mean $\sigma_{\rm CCF}$ and its standard deviation, if the star is measured more than twice. The last two lines of this table give, for each night, the mean and the standard deviation of the $\sigma_{\rm CCF}$ for the red giant sample only, which are marked in this table with an asterisk. However, these means and standard deviations are not significantly different from those computed by taking into account all of the stars, i.e., including dwarfs and subgiants.

Unexpectedly, the mean of the $\sigma_{\rm CCF}$ obtained during the first night (July 6) is significantly higher than the mean of the

Table 3. Radial velocities of all standard stars measured in December 1990 and January 1991.

HD	V_r^{COR}	Dec 21	Dec 22	Dec 23	Dec 24	Dec 25	Dec 26	Jan 26	$\overline{V}_r^{CAS}$
	(km s^{-1})	..... $V_r^{CAS}-V_r^{COR}$ (km s^{-1})							(km s^{-1})
(1)	(2)	(3)	(4)	(5)	(6)	(7)	(8)	(9)	(10)
CORAVEL radial velocity standards									
6655	19.4±0.3	−0.4	...	...	...	...	...	...	19.0
21197	−13.8±0.2	...	...	1.7	0.6	−0.2	...	...	−13.1±1.0
24916a	3.2±0.3	...	−0.4	...	...	...	...	−0.3	2.9
32147	20.9±0.3	...	0.3	...	...	...	...	...	21.2
65277a	−4.7±0.3	...	...	−1.0	0.3	...	...	...	−5.1
NGC 2447									
4	23.2±0.2	0.9	...	−0.4	...	0.3	0.2	−0.3	23.4±0.5
28	21.2±0.1	...	...	0.4	...	0.7	0.4	−0.0	21.6±0.3
34	22.2±0.2	1.3	...	−0.2	...	1.7	−0.1	0.1	22.7±0.8
71	21.9±0.2	...	...	−1.2	...	...	...	...	20.7
85	20.7±0.2	...	...	0.0	...	...	...	...	20.7
NGC 2682									
84	33.8±0.2	...	0.9	...	−0.1	...	...	1.1	34.4±0.6
141	33.4±0.6	...	−0.3	...	1.0	...	...	−0.1	33.5±0.7
151	33.6±0.5	...	−0.0	...	1.2	...	...	...	34.2
266	34.2±0.2	...	−1.7	...	...	...	...	...	32.5
Metal deficient halo giants									
23798	89.1±0.3	−0.4	...	...	...	...	−1.0	...	88.4
24418	94.7±0.3	...	...	...	...	...	−1.4	...	93.3
33771	−13.6±0.4	...	...	...	...	−1.1	...	...	−14.7
37828	194.2±0.2	...	...	...	...	...	0.8	...	195.0
38893	128.3±0.3	−1.5	...	...	...	...	...	...	126.8
83212	108.7±0.3	...	−0.7	...	−0.1	...	...	−1.1	108.1±0.5
93529	145.4±0.3	...	...	...	−0.1	0.1	...	...	145.4
103295	3.0±0.3	...	...	...	1.3	...	...	...	4.3
Mean		0.0	−0.3	−0.1	0.5	0.2	−0.2	−0.1	...
σ_{n-1}		1.1	0.8	1.0	0.6	0.9	0.8	0.7	...

Table 4. σ_{CCF} of the standard stars measured in July 1989.

HD	Sp Type	Jul 6	Jul 7	Jul 8	$\overline{\sigma}_{CCF}$
		..... σ_{CCF} (km s^{-1})			(km s^{-1})
(1)	(2)	(3)	(4)	(5)	(6)
107328*	K1 IIIb	...	6.76	6.88	...
126053	G1 V	6.89	6.64	6.74	6.76±0.13
136202	F8 IV-V	7.23	...	...	...
171391*	G8 III	7.24	6.90	6.93	7.02±0.19
182572	G7 IV	...	...	6.71	...
187691	F8 V	7.28	7.02	7.00	7.10±0.16
203638*	K0 III	7.09	6.82	6.76	6.89±0.18
223311*	K4 III	7.38	...	...	...
111417	K3 IV	7.18	6.58	6.82	6.92±0.23
193231	G8 V	...	...	6.72	...
196983*	K2 III	...	...	6.79	...
219509	K5 V	...	...	6.93	...
Mean		7.24	6.83	6.84	...
σ_{n-1}		0.15	0.07	0.08	...

* giant stars taken into account to compute the mean and the σ_{n-1} of the σ_{CCF}.

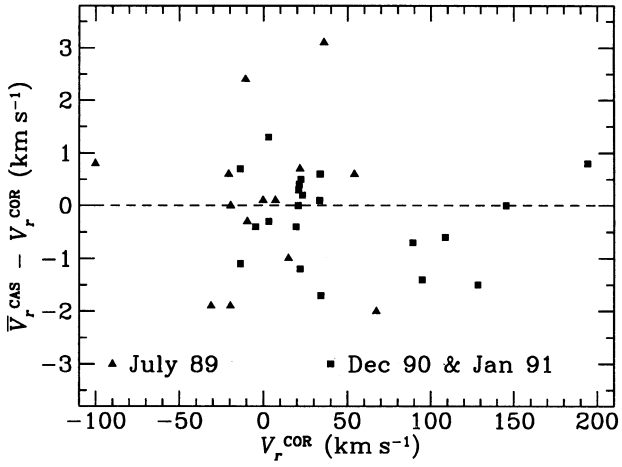

Fig. 3. Differences between the present and the CORAVEL V_r as a function of the CORAVEL V_r.

σ_{CCF} obtained during the other two nights (July 7 and 8). This is also apparent in Fig. 4 which shows with a dashed line the histogram of all σ_{CCF} measurements obtained during July 6 and with a solid line the histogram of all the σ_{CCF} measurements

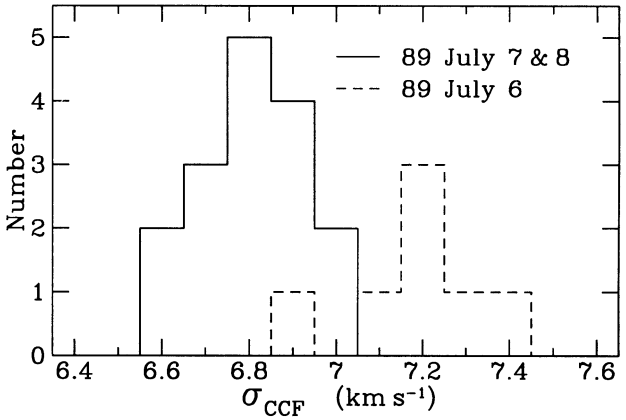

Fig. 4. Histogram of the standard deviations σ_{CCF} of the CCFs of the standard star spectra obtained in July 1989.

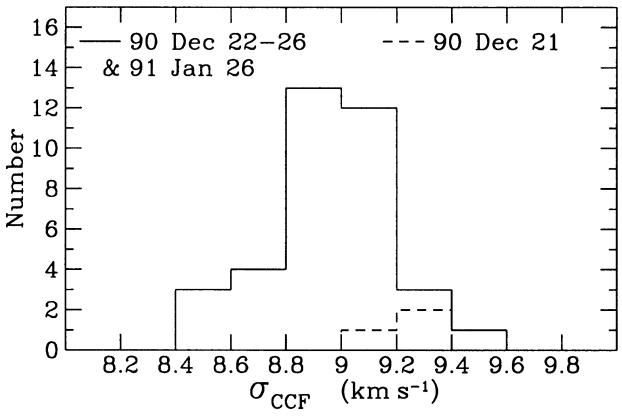

Fig. 5. Histogram of the standard deviations σ_{CCF} of the CCFs of the standard star spectra obtained in December 1990 and January 1991.

obtained during July 7 and 8. This difference is possibly related to small changes in the slit width and in the seeing value between the different nights. Within one night, the σ_{CCF} variations from star to star are small, as is expected since σ_{CCF} depends mostly on the instrumental resolution, which is lower than the intrinsic resolution of the stellar spectra.

The σ_{ref} derived to compute the present globular cluster velocity dispersions from Eq. (2) are $\sigma_{ref} = 7.2 \pm 0.15$ km s^{-1} for July 6 and $\sigma_{ref} = 6.8 \pm 0.1$ km s^{-1} for July 7 and 8.

4.2.2. σ_{ref} from December 1990 and January 1991

For each standard star observed in December 1990 and January 1991, Table 5 displays in column (1) the identification number of the star observed, in column (2) its spectral type, in column (3) its metallicity, in columns (4) to (10) the σ_{CCF} measurements obtained during the different nights, and in column (11) the mean σ_{CCF} and its its standard deviation, if the star is measured more than twice. The last two lines of this table give, for each night, the mean and the standard deviation of the σ_{CCF} measurements from all standard stars (all of them are giants).

For this second observing run, we find no significant variation in the mean σ_{CCF} from night to night. The mean σ_{CCF} from the first night measurements (Dec 21) is only marginally higher than the ones from the measurements of the other 6 nights. Fig. 5 displays, with a dashed line, the histogram of the σ_{CCF} measurements made during the first night and, with a solid line, the histogram of σ_{CCF} made during the other 6 nights. The repeatability of our σ_{CCF} measurements is very good: the standard deviations of the measurements of standard stars (see Table 5) are smaller than 0.25 km s^{-1} and the σ_{CCF} variations from star to star are similarly small. As for the first run, this reflects the fact that σ_{CCF} depends mostly on the instrumental resolution.

The value $\sigma_{ref} = 9.0 \pm 0.2$ km s^{-1} is used to compute the globular cluster velocity dispersions from this second run. The above value and uncertainty are simply the mean and the standard deviation of all of the σ_{CCF} values obtained during this second observing run, i.e., all of the σ_{CCF} values given in Table 5. As a check, σ_{CCF} is evaluated in a similar way for a spectrum of a red giant star in the Fornax dwarf spheroidal and a spectrum of a red giant star in the Galactic globular cluster NGC 4833. The resulting values are 9.0 km s^{-1} and 8.9 km s^{-1}, respectively, which match perfectly the above σ_{ref} value.

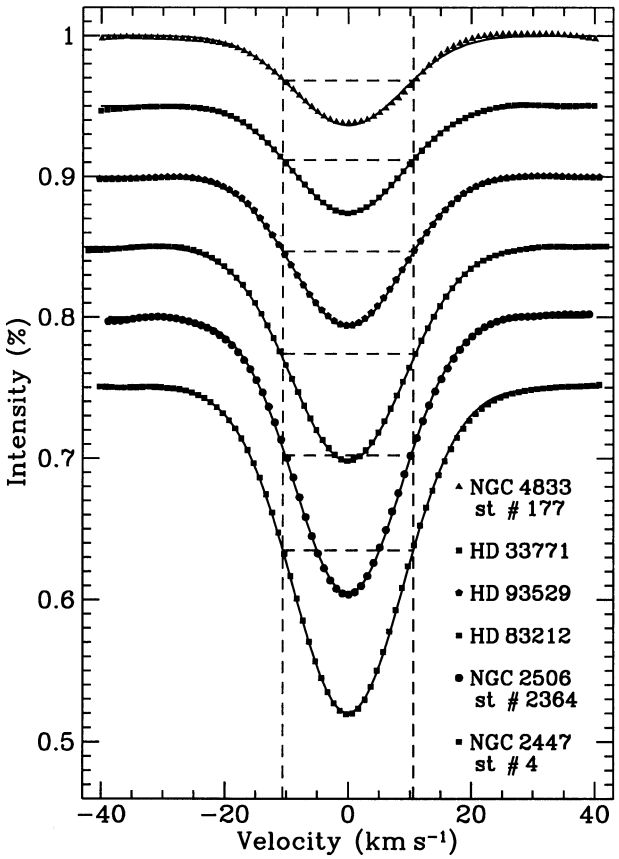

Fig. 6. CCFs of giant stars of metallicities ranging from (top) −2 dex (star No. 177 in the Galactic globular cluster NGC 4833) to (bottom) the solar value (star No. 4 in the open cluster NGC 2447).

Table 5. σ_{CCF} of the standard stars measured in December 1990 and January 1991.

	Sp Type	[Fe/H]	Dec 21	22	23	24	25	26	Jan 26	$\overline{\sigma}_{CCF}$
			..... σ_{CCF} ($km\,s^{-1}$)							($km\,s^{-1}$)
(1)	(2)	(3)	(4)	(5)	(6)	(7)	(8)	(9)	(10)	(11)
Giant stars in the open cluster NGC 2447										
4	...	0.0	9.32	...	8.98	...	9.05	9.01	9.17	9.11±0.14
28	...	0.0	...	...	8.79	...	9.14	8.99	9.02	8.99±0.15
34	...	0.0	9.52	...	9.12	...	9.10	9.08	9.14	9.19±0.18
71	...	0.0	...	...	8.86	...	...	...	...	8.86
85	...	0.0	...	...	9.07	...	...	...	...	9.07
Giant stars in the open cluster NGC 2506										
1229	...	−0.6	...	...	...	...	...	8.63	...	8.63
2364	...	−0.6	...	...	...	...	...	8.68	8.80	8.74
Giant stars in the open cluster NGC 2682										
84	...	−0.1	...	8.91	...	9.03	...	...	8.56	8.83±0.24
141	K0 III	−0.1	...	9.00	...	8.91	...	...	8.60	8.84±0.21
151	K0 III	−0.1	...	8.86	...	8.87	...	...	...	8.87
266	K1 III	−0.1	...	8.96	...	...	...	...	...	8.96
Metal deficient halo stars										
23798	K1 III	−2.3	9.36	...	...	...	...	9.31	...	9.34
24418	...	−1.4	...	...	...	...	...	8.58	...	8.58
33771	G7 III	−2.6	...	...	...	...	8.91	...	...	8.91
37828	...	−1.5	...	...	...	...	...	8.76	...	8.76
38893	G3 III	−1.9	9.16	...	...	...	...	...	...	9.16
83212	K0 III	−1.8	...	9.53	...	9.27	...	...	9.37	9.39±0.13
93529	G7 III	−2.0	...	...	...	8.99	9.03	...	...	9.01
103295	G5 III	−1.7	...	...	...	8.85	...	...	...	8.85
Mean			9.34	9.05	8.96	8.99	9.05	8.88	8.95	...
σ_{n-1}			0.15	0.27	0.14	0.16	0.09	0.27	0.30	...

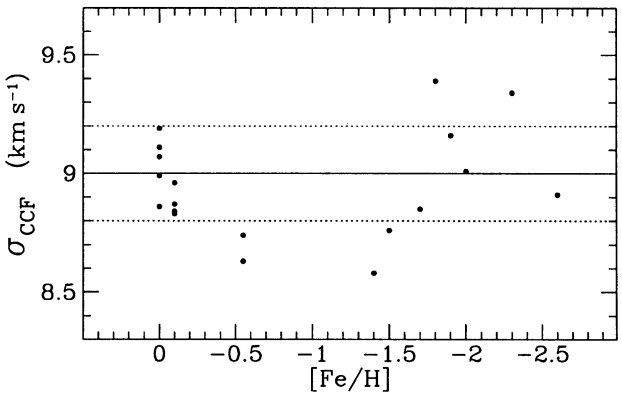

Fig. 7. σ_{CCF} as a function of the star metallicity, from the measurements of the second observing run. The continuous and dotted horizontal lines represent the σ_{ref} value and its uncertainty, as derived from the measurements of the second observing run (see Sect. 4.2.2).

4.2.3. Independence of σ_{CCF} from the star metallicity

The velocity dispersion estimates derived from Eq. (2) are biased if the σ_{ref} values derived from our samples of standard stars are not representative of the σ_{CCF} values of the typical globular cluster stars. Such a bias could arise if σ_{CCF} depended on stellar metallicity. Since the globular clusters in our sample span a considerable metallicity range, a check of such a possible dependence is needed.

In the case of CORAVEL, our extensive experience shows that σ_{CCF} is independent of stellar metallicity. The measurements, during our second observing run, of a few metal-weak halo giants – see Table 5 – allow us to confirm that, in the present study, σ_{CCF} is also completely independent of stellar metallicity. This appears clearly in both Figs. 6 and 7. The former presents a sequence of CCFs of stars of increasing metallicity (from top to bottom) but of equal widths (dashed lines). The latter displays σ_{CCF} as a function of the metallicity, for all stars measured during our second observing run (Table 5), and confirms the lack of relation between these two quantities. It is worth mentioning that the metallicity range of the stars in our sample encompasses the metallicity range of the studied globular clusters.

5. Cluster radial velocities and core velocity dispersions

Some of the cross-correlation functions (CCFs) obtained from the globular cluster integrated-light spectra are displayed in Figs. 8 and 9. Tables 6 and 7 give, for each cluster spectrum obtained, in column (1) the observation number from Table 1, in column (2) the NGC number of the cluster, in column (3) the derived heliocentric radial velocity V_r and its uncertainty, in column (4) the standard deviation σ_{CCF} of the CCF and its uncertainty, in column (5) the relative depth D of the CCF, in

column (6) the signal-to-noise ratio (S/N) of the spectrum, in column (7) the uncertainty ε of V_r and $\sigma_{\rm CCF}$ due to the spectrum noise, in column (8) the value used for the intrinsic standard deviation $\sigma_{\rm ref}$ from the standard CCFs, as determined in Sect. 4.2, in column (9) the projected velocity dispersion in the cluster core $\sigma_p^{\rm obs}$ (core), derived from Eq. (2), with its uncertainty due to the instrumental error and to the spectrum noise, in column (10) the statistical error due to the small sample of bright stars observed through the slit (see Sect. 6), and in column (11) the projected velocity dispersion in the cluster core σ_p (core) and its uncertainty, both including the contribution from the statistical error simulations. The S/N ratio given in column (6) for each spectrum is calculated as follows: the mean value of the spectrum continuum – i.e., the signal S – is derived from the continuum of the unnormalized CCF and the noise N is computed from the photon counting and the CCD readout noises (see Dubath et al. 1990 for more details).

Fig. 10 displays the histogram of the core velocity dispersion values for the Galactic and Magellanic clusters, along with the core velocity dispersions for three Fornax globular clusters taken from Dubath et al. (1992).

5.1. Radial velocity measurement accuracy

In order to estimate the uncertainties of our radial velocities, we proceed in two steps. First, the contribution from instrumental problems is estimated by using our standard star measurements. In Sect. 4.1, instrumental radial velocity uncertainties equal to 1.6 and 0.8 $\rm km\,s^{-1}$ are estimated for the first and the second observing runs, respectively. In those cases, the influence of the noise is negligible because of the high S/N ($\sim$ 30–50) ratio of the standard-star spectra. Second, the additional uncertainty ε, arising from spectrum noise, in the case of lower S/N spectra, is estimated by using a generalization of Eq. (3) from Dubath et al. (1990), i.e.,

$$\varepsilon = \frac{5}{D\ {\rm S/N}\ (N_{\rm lines})^{1/2}}\ {\rm km\,s^{-1}}\ , \qquad (3)$$

where S/N is the signal-to-noise ratio of the spectrum, D is the relative depth of the cross-correlation function, and $N_{\rm lines}$ is the number of spectral lines present in the cross-correlation template (typically from about 800 to 1200 lines in the present study, depending on the wavelength range of the spectrum). This formula is derived from about two thousand numerical simulations (Dubath et al. 1990). For each simulation, a random-noise frame is generated and added to a raw CCD frame of a bright standard star in order to reproduce the photon counting noise and the readout noise present in a low S/N CCD frame. Each of these frame is fully reduced in the standard way used for our observations. The reduced spectra are cross-correlated and the resulting CCFs fitted by Gaussians. The expression giving ε (Eq. (3)) is derived from the behavior of the scatter of the resulting Gaussian parameters (V_r and $\sigma_{\rm CCF}$) as a function of the simulation parameters (S/N, D). In all cases, the standard deviation of the resulting V_r is similar to the standard deviation of the resulting $\sigma_{\rm CCF}$. Consequently, the above formula provides the uncertainty due to the spectrum noise for the V_r as well as for the $\sigma_{\rm CCF}$ determinations. The derived ε values are listed in column (7) of Tables 6 and 7.

The two kinds of errors (instrumental and noise) are independent and their distributions are roughly Gaussian. The final radial velocity uncertainty, given in column (3) of Tables 6 and 7, is the square root of the quadratic sum of both errors, i.e., $(1.6^2+\varepsilon^2)^{1/2}$ and $(0.8^2+\varepsilon^2)^{1/2}$, for the first and second observing runs, respectively.

5.2. Velocity-dispersion measurement accuracy

The uncertainty of the standard deviation, $\sigma_{\rm CCF}$, of a cluster CCF is also given by the combination of the instrumental uncertainty and that due to the spectrum noise, ε. The instrumental uncertainty of the $\sigma_{\rm CCF}$ measurements is similar to the uncertainty of the $\sigma_{\rm ref}$ values (listed in column (8) of Tables 6 and 7), since $\sigma_{\rm ref}$ is the mean $\sigma_{\rm CCF}$ of the CCFs of standard stars, for which the uncertainty due to the spectrum noise is negligible because of the high S/N of their spectra.

The uncertainty of $\sigma_{\rm CCF}$ given in column (4) of Tables 6 and 7 is the square root of the quadratic sum of the $\sigma_{\rm ref}$ uncertainty and of the ε value. In order to compute the uncertainties of the velocity dispersion $\sigma_p^{\rm obs}$, given in column (9) of Tables 6 and 7, the uncertainties of both $\sigma_{\rm CCF}$ and $\sigma_{\rm ref}$ are taken into account (see Eq. (2)).

6. Statistical errors on the σ_p measurements due to the small samples of stars predominant in luminosity

The stellar luminosity function in a globular cluster decreases sharply with increasing luminosity. The relative contribution of a given group of stars (e.g., defined by an interval in V magnitude) to the integrated light of a globular cluster can be estimated from the luminosity function of the cluster and the typical stellar luminosity of the group. The result shows that the contribution in luminosity of the few brightest stars is of the same order of magnitude as the contribution of the much more numerous fainter stars. Therefore, the few brightest stars lying in a small area of integration can easily dominate the integrated light, and then bias the velocity-dispersion estimate. There are two extreme cases: on one hand, if the brightest star in the spectrograph slit dominates completely the integrated light, the CCF will nearly have a stellar narrow profile and the velocity dispersion will be underestimated; on the other hand, if the few dominant stars have unusually large radial velocity differences, the CCF is artificially broadened, leading to overestimates of the velocity dispersion.

6.1. Numerical simulations of integrated-light CCFs

Extensive numerical simulations have been carried out in order to quantitatively estimate the influence of statistical errors due to small samples of stars on our radial velocity and velocity dispersion determinations.

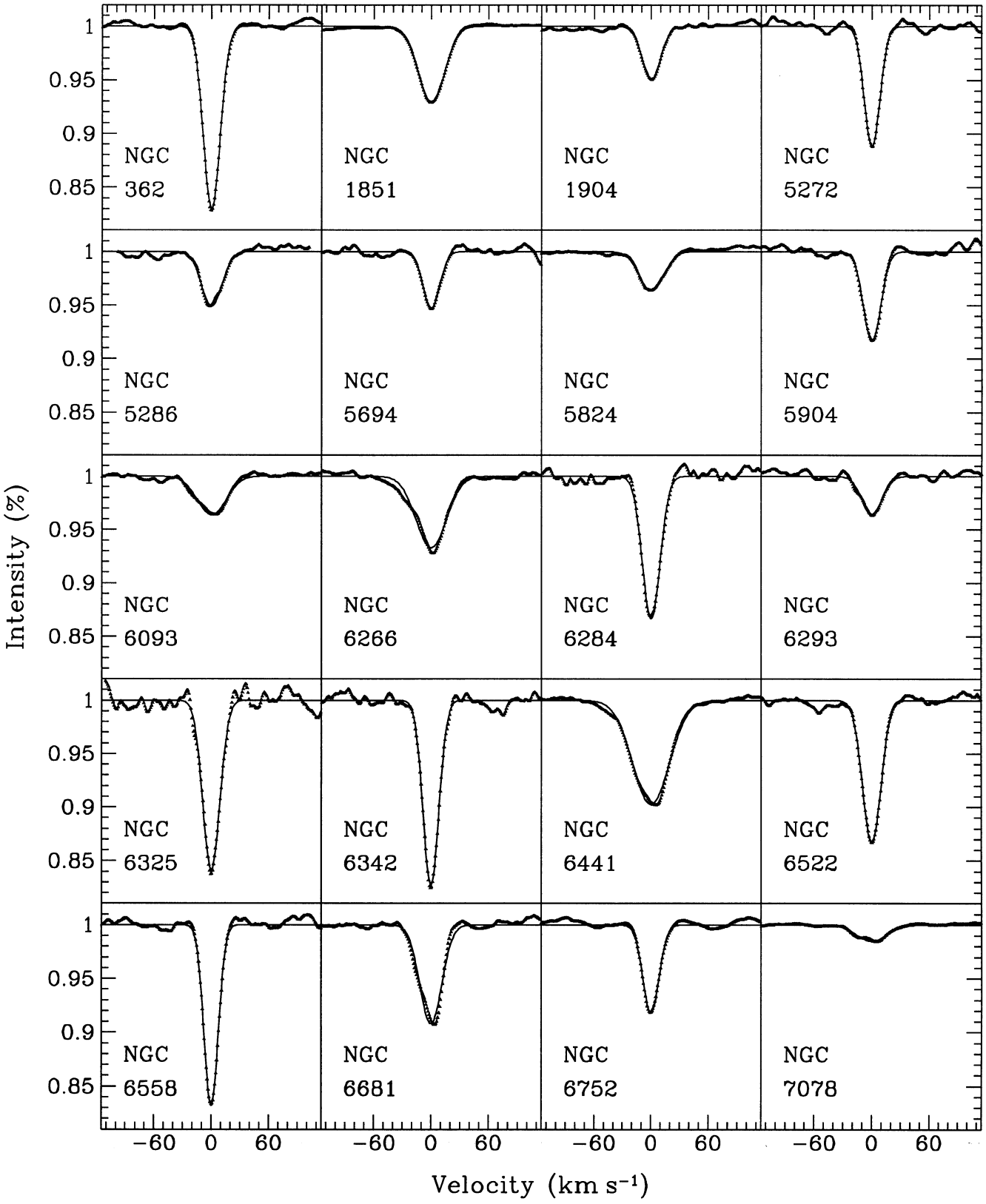

Fig. 8. CCFs of the integrated light-spectra of some of the Galactic globular clusters.

Table 6. Radial velocities and core velocity dispersions for all Galactic globular clusters in our sample.

Obs No. (1)	NGC No. (2)	V_r ($\mathrm{km\,s^{-1}}$) (3)	σ_{CCF} ($\mathrm{km\,s^{-1}}$) (4)	D (%) (5)	S/N (6)	ε ($\mathrm{km\,s^{-1}}$) (7)	σ_{ref} ($\mathrm{km\,s^{-1}}$) (8)	σ_p^{obs}(core) ($\mathrm{km\,s^{-1}}$) (9)	stat err ($\mathrm{km\,s^{-1}}$) (10)	σ_p(core) ($\mathrm{km\,s^{-1}}$) (11)
1	104	−19.4±1.6	11.8±0.2	0.110	13.0	0.12	7.2±0.15	$9.3^{+0.4}_{-0.4}$	$+4.8:_{-2.6}$	$10.0^{+4.8:}_{-2.6}$
2	"	−19.9±1.6	11.5±0.2	0.107	13.0	0.12	6.8±0.10	$9.3^{+0.3}_{-0.3}$	...	...
3	362	223.3±1.6	8.9±0.1	0.171	14.0	0.07	6.8±0.10	$5.7^{+0.3}_{-0.3}$	$+3.0:_{-1.6}$	$6.2^{+3.0:}_{-1.6}$
4	1851	320.3±0.8	13.8±0.2	0.071	59.8	0.04	9.0±0.20	$10.5^{+0.4}_{-0.5}$	$+2.5_{-1.7}$	$11.3^{+2.5}_{-1.8}$
5	1904	200.6±0.9	9.7±0.3	0.050	15.4	0.19	9.0±0.20	$3.6^{+1.1}_{-1.6}$	$+1.9:_{-1.0}$	$3.9^{+2.2:}_{-1.9}$
6	5272	−146.3±1.6	8.1±0.3	0.112	5.0	0.30	6.8±0.10	$4.4^{+0.7}_{-0.8}$	$+2.3:_{-1.2}$	$4.8^{+2.4:}_{-1.4}$
7	5286	57.2±1.7	10.8±0.7	0.050	5.0	0.67	7.2±0.15	$8.0^{+1.0}_{-1.1}$	$+4.2:_{-2.2}$	$8.6^{+4.3:}_{-2.5}$
8	5694	−142.7±1.7	8.8±0.5	0.053	6.4	0.49	6.8±0.10	$5.6^{+0.9}_{-1.0}$	$+1.3_{-1.3}$	$6.1^{+1.3}_{-1.3}$
9	5824	−26.0±1.6	12.6±0.3	0.037	16.0	0.28	6.8±0.10	$10.6^{+0.4}_{-0.4}$	$+1.6_{-1.6}$	$11.1^{+1.6}_{-1.6}$
10	5904	54.7±1.6	9.1±0.3	0.084	6.0	0.33	6.8±0.10	$6.0^{+0.6}_{-0.7}$	$+3.1:_{-1.7}$	$6.5^{+3.2:}_{-1.8}$
11	5946	129.1±1.9	8.1±1.1	0.101	1.5	1.10	7.2±0.15	$3.7^{+2.2}_{-2.7}$	$+1.9:_{-1.0}$	$4.0^{+2.9:}_{-2.9}$
12	6093	7.8±1.7	15.0±0.5	0.037	10.0	0.45	6.8±0.10	$13.4^{+0.6}_{-0.6}$	$+7.0:_{-3.8}$	$14.5^{+7.0:}_{-3.8}$
13	6256	−104.6±3.1	9.5±2.6	0.081	0.8	2.57	6.8±0.10	$6.6^{+3.4}_{-6.0}$	$+3.4:_{-1.8}$	...
14	6266	−71.8±1.6	16.0±0.3	0.067	10.0	0.25	7.2±0.15	$14.3^{+0.4}_{-0.4}$	$+7.4:_{-4.0}$	$15.4^{+7.4:}_{-4.0}$
15	6284	27.5±1.7	9.3±0.4	0.134	3.0	0.42	6.8±0.10	$6.3^{+0.7}_{-0.8}$	$+3.3:_{-1.8}$	$6.8^{+3.4:}_{-2.0}$
16	6293	−147.9±1.8	10.5±0.8	0.037	5.5	0.82	7.2±0.15	$7.6^{+1.2}_{-1.4}$	$+4.0:_{-2.1}$	$8.2^{+4.2:}_{-2.5}$
17	6325	31.0±1.8	9.0±0.8	0.157	1.4	0.76	6.8±0.10	$5.9^{+1.2}_{-1.4}$	$+3.1:_{-1.7}$	$6.4^{+3.3:}_{-2.2}$
18	6342	118.0±1.6	8.3±0.3	0.172	3.2	0.30	6.8±0.10	$4.8^{+0.7}_{-0.7}$	$+2.5:_{-1.3}$	$5.2^{+2.6:}_{-1.5}$
19	6397	15.1±1.6	7.5±0.3	0.045	13.0	0.28	7.2±0.15	$2.1^{+1.3}_{-2.1}$	$+1.1:_{-0.6}$	...
20	"	15.0±1.6	7.4±0.4	0.050	10.0	0.33	7.2±0.15	$1.7^{+1.5}_{-1.7}$	...	...
21	6441	14.6±1.6	19.3±0.2	0.098	12.0	0.14	6.8±0.10	$18.1^{+0.2}_{-0.2}$	$+9.4:_{-5.1}$	$19.5^{+9.4:}_{-5.1}$
22	6522	−10.3±1.6	9.6±0.3	0.133	4.3	0.29	6.8±0.10	$6.8^{+0.5}_{-0.6}$	$+3.5:_{-1.9}$	$7.3^{+3.5:}_{-2.0}$
23	6558	−198.8±1.6	7.5±0.2	0.168	5.6	0.18	6.8±0.10	$3.2^{+0.6}_{-0.8}$	$+1.7:_{-0.9}$	$3.5^{+1.8:}_{-1.2}$
24	6681	223.4±1.6	11.5±0.3	0.092	7.4	0.24	6.8±0.10	$9.3^{+0.4}_{-0.4}$	$+4.8:_{-2.6}$	$10.0^{+4.8:}_{-2.6}$
25	6752	−32.0±1.6	8.5±0.2	0.082	21.0	0.10	7.2±0.15	$4.5^{+0.5}_{-0.6}$	$+2.3:_{-1.3}$	$4.9^{+2.4:}_{-1.4}$
26	7078	−111.3±1.6	15.6±0.2	0.015	54.0	0.21	6.8±0.10	$14.0^{+0.3}_{-0.3}$	$+5.0_{-3.0}$	$15.1^{+5.0}_{-3.0}$
27	7099	−180.7±1.8	8.2±0.8	0.022	11.0	0.83	6.8±0.10	$4.6^{+1.5}_{-2.0}$	$+2.8:_{-1.5}$	$5.8^{+2.9:}_{-1.7}$
28	"	−181.1±1.8	8.6±0.9	0.020	11.0	0.91	6.8±0.10	$5.3^{+1.5}_{-1.9}$	...	...
29	"	−183.6±2.2	8.9±1.5	0.017	8.0	1.47	6.8±0.10	$5.7^{+2.2}_{-3.0}$	...	...
30	"	−185.1±1.7	8.9±0.5	0.031	14.4	0.45	6.8±0.10	$5.7^{+0.8}_{-0.9}$	...	...
31	"	−182.9±2.7	8.2±2.2	0.017	5.4	2.18	6.8±0.10	$4.6^{+3.3}_{-3.6}$	...	...

By definition, an integrated-light spectrum is the sum of all the spectra of the stars which appear inside the area of integration in projection on the plane of the sky. Such a spectrum may be reproduced, numerically, by adding stellar spectra of appropriate spectral types, each of them shifted in wavelength by a small amount in order to mimic the spatial random motions of the stars. Such simulations have been carried out by Zaggia et al. (1992, 1993) in the cases of the two Galactic globular clusters M30 and M15. Alternatively, the CCFs of integrated-light spectra may be directly simulated by adding stellar CCFs adequately shifted in velocity (Dubath et al. 1994). Within the framework of our cross-correlation technique, the CCF of our digital mask with a sum of spectra is equivalent to the sum of the CCFs of the mask with each spectrum. Since our cross-correlation technique produces CCFs which are nearly perfect Gaussians (see Fig. 6), we simply add Gaussian functions to reproduce CCFS of integrated-light spectra. Our simulations have first been applied to the case of the Galactic globular cluster M15 – the prototype of the collapsed globular cluster – in order to point out the difficulties in measuring the central velocity dispersion in this cluster. The results as well as some details on our numerical simulations are presented in Dubath et al. (1994).

In order to simulate one integrated-light CCF, we proceed as follow:

1. An absolute V magnitude and a $B-V$ color index are attributed to a simulated globular cluster star according to an observed color-magnitude diagram and luminosity function of a real globular cluster. A radial velocity V_r^{star} is randomly assigned

Table 7. Radial velocities and core velocity dispersions for all Magellanic globular clusters in our sample.

Obs No. (1)	NGC No. (2)	V_r (km s^{-1}) (3)	σ_{CCF} (km s^{-1}) (4)	D (%) (5)	S/N (6)	ε (km s^{-1}) (7)	σ_{ref} (km s^{-1}) (8)	σ_p^{obs}(core) (km s^{-1}) (9)	stat err (km s^{-1}) (10)	σ_p(core) (km s^{-1}) (11)
SMC globular cluster										
32	121	S/N too low!								
33	"	146.9±2.0	8.8±1.0	0.095	1.8	0.98	7.2±0.1	$5.1^{+1.7}_{-2.4}$	$^{+1.3}_{-1.3}$	$5.9^{+2.1}_{-2.7}$
34	419	188.3±0.9	9.5±0.3	0.113	4.8	0.28	9.0±0.2	$3.2^{+1.3}_{-3.2}$	$^{+0.8}_{-0.8}$	...
LMC globular clusters										
35	1466	203.6±1.1	9.8±0.8	0.046	4.3	0.76	9.0±0.2	$3.8^{+2.0}_{-3.8}$	$^{+2.0:}_{-1.1}$	...
36	1754	234.2±0.9	11.6±0.3	0.052	10.5	0.28	9.0±0.2	$7.2^{+0.8}_{-0.8}$	$^{+3.7:}_{-2.0}$	$7.8^{+3.8:}_{-2.2}$
37	1786	262.6±0.9	12.0±0.4	0.041	9.4	0.39	9.0±0.2	$7.9^{+0.9}_{-0.9}$	$^{+1.2}_{-1.2}$	$8.3^{+1.5}_{-1.5}$
38 39	1835	195.3±0.9	12.8±0.3	0.050	18.0	0.22	7.8±0.2	$10.1^{+0.5}_{-0.5}$	$^{+1.3}_{-1.3}$	$10.4^{+1.4}_{-1.4}$
40	"	192.1±0.9	13.8±0.3	0.035	21.1	0.20	9.0±0.2	$10.5^{+0.5}_{-0.6}$	...	...
41	1916	267.6±0.8	12.1±0.2	0.062	32.8	0.07	9.0±0.2	$8.0^{+0.5}_{-0.6}$	$^{+1.0}_{-1.0}$	$8.2^{+1.1}_{-1.2}$
42	"	266.6±0.8	12.0±0.2	0.059	21.6	0.12	9.0±0.2	$7.9^{+0.6}_{-0.6}$	...	...
43	2005	273.5±0.8	11.9±0.2	0.054	21.4	0.13	9.0±0.2	$7.7^{+0.6}_{-0.6}$	$^{+1.2}_{-1.2}$	$8.1^{+1.3}_{-1.3}$
44	2019	279.5±0.8	11.5±0.2	0.072	20.4	0.10	9.0±0.2	$7.2^{+0.6}_{-0.6}$	$^{+1.1}_{-1.1}$	$7.5^{+1.3}_{-1.3}$
45	2210	338.6±0.9	11.2±0.3	0.048	14.5	0.22	9.0±0.2	$6.6^{+0.7}_{-0.8}$	$^{+1.5}_{-1.5}$	$7.3^{+1.7}_{-1.7}$
46	Ho 11	244.5±0.9	8.5±0.5	0.056	6.5	0.41	9.0±0.2	...	...	...

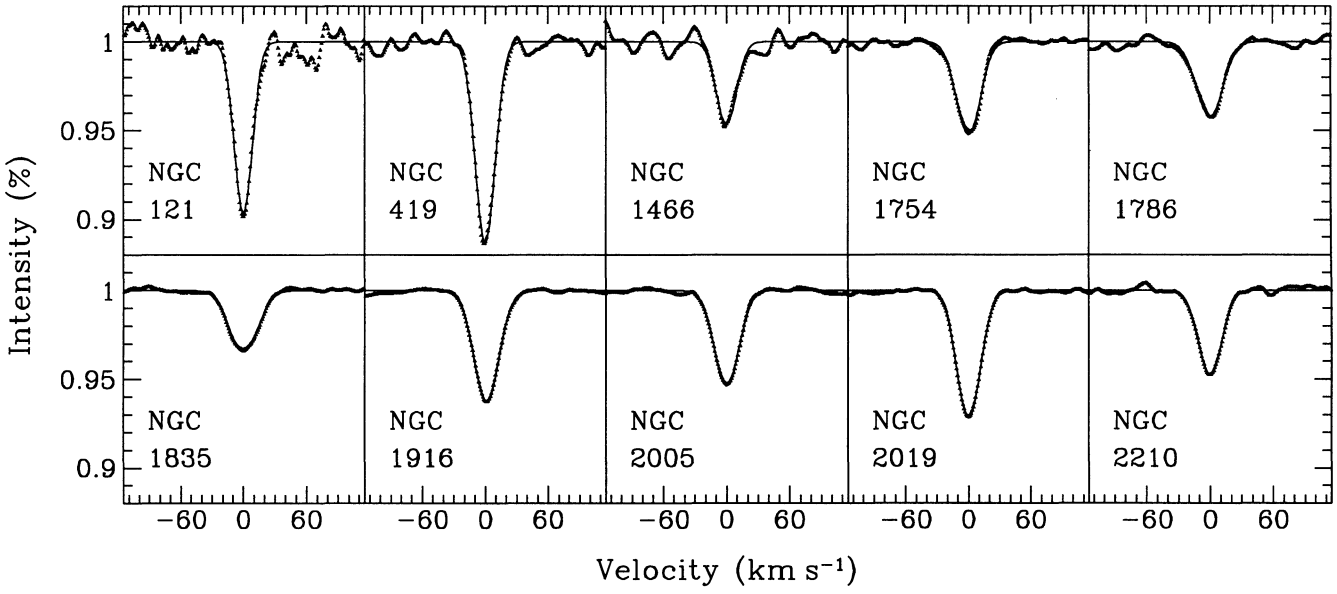

Fig. 9. CCFs of the integrated-light spectra of 10 Magellanic globular clusters.

to this star from a Gaussian distribution of standard deviation σ_{in}, which is the input velocity dispersion of the simulation.

2. Assuming that the CCF of the star is Gaussian, it can be computed from the following equation,

$$\mathrm{CCF(v)} = 10^{\frac{-M_V}{2.5}} \left\{ 1 - D_{\mathrm{CCF}} \exp\left[-\frac{(V_r^{\mathrm{star}} - v)^2}{2\sigma_{\mathrm{ref}}^2} \right] \right\} \qquad (4)$$

where σ_{ref} is the typical standard deviation of the CCF of individual standard stars (see Sect. 4.2) and D_{CCF} is a function of the $B-V$ color index – the redder the star, the deeper its CCF – (Dubath et al. 1994).

3. The CCFs of N stars are summed together in order to reproduced the CCF of an integrated-light spectrum. N is chosen so that, on average, the total magnitude of N stars matches the magnitude M_V^{int} of the observed light integrated over the considered aperture. In order to take into account some statistical variation in the number N of added stellar CCFs, N is not constant from one simulation to another. For each simulated integrated-light CCF, the number of added stars is taken from a

Gaussian distribution of mean and standard deviation equal to N and $\sqrt{N}$, respectively.

4. As in the case of the CCF of an observed integrated-light spectrum, a Gaussian is fitted to the sum of the simulated stellar CCFs in order to derive V_r and $\sigma_{\rm CCF}$. The output velocity dispersion resulting from the simulation is given by $\sigma_{\rm out} = (\sigma^2_{\rm CCF} - \sigma^2_{\rm ref})^{1/2}$.

6.2. Ingredients of the simulations

In addition to the simulations adapted to the case of M15 (Dubath et al. 1994), some simulations using the color-magnitude diagram of 47 Tuc (Hesser & Hartwick 1977, Hesser et al. 1987) and the color-magnitude diagram of M3 (Buonanno et al. 1988 and private communication) have been carried out. The color-magnitude diagrams of the metal-rich globular cluster 47 Tuc and of the metal-poor globular cluster M15 are at two extremities in terms of CMD morphology (see, e.g., Fig. 21 of Hesser et al. 1987). In 47 Tuc, the fiducial sequences are redder with an extremely red horizontal branch. In M15, the same fiducial sequences are bluer with a horizontal branch extending from the red to the blue. The color-magnitude diagram of M3 is complete down to about a V magnitude of 21 and contains the measurements of more than 10,000 stars. The properties of M3, in terms of metal content, color-magnitude diagram morphology and luminosity function are intermediate to 47 Tuc and M15, i.e., more representative of a "typical" globular cluster. For this reason, all results of simulations presented in this section are derived from the simulations carried out with the M3 color-magnitude diagram. However, the three kinds of simulations – using color-magnitude diagrams of M15, M3 and 47 Tuc – are used to check that our results and conclusions do not depend significantly on the morphology of the particular color-magnitude diagram used.

Another ingredient of the simulations is the total absolute magnitude $M_V^{\rm int}$ of the integrated light through the slit. $M_V^{\rm int}$ is first estimated, for many Galactic and some LMC globular clusters, from the published central surface brightness values taken from Webbink (1985) and Mateo (1987). These values are used to calibrate the mean flux in the continuum of the integrated light spectra. This is done by determining the constant C in the equation $M_V^{\rm int} = C - 2.5\log(\text{flux})$. Fig. 11 presents, for the LMC and Galactic globular clusters, the relation $M_V^{\rm int}$ (from the above formula) as a function of $M_V^{\rm int}$ (from the central surface brightness). The standard deviation of the points around the best fit is < 0.4 magnitude. Using this relation, $M_V^{\rm int}$ can be derived from the mean flux of the integrated-light spectrum of any of our clusters, with an accuracy of about $\pm 40\%$.

6.3. Results of the simulations

In a given simulation, $\sigma_{\rm in}$ represents the genuine cluster velocity dispersion, while $\sigma_{\rm out}$ corresponds to the observed velocity dispersion $\sigma_p^{\rm obs}$. In order to estimate the uncertainty of the observed velocity dispersion, we proceed as follows. The first parameter used for the simulation is the absolute magnitude $M_V^{\rm int}$ of the integrated light in the aperture, which fixes the number N of stellar CCFs to be added. For a given $M_V^{\rm int}$, i.e., for a given N, we consider a set of values of input velocity dispersions $\sigma_{\rm in}$, ranging from 1 to 26 km s^{-1} with a step of 1 km s^{-1}. For each $\sigma_{\rm in}$, 5000 simulated CCFs are computed, following the above 4 steps in Sect. 6.1. The number of times that the standard deviation $\sigma_{\rm out}$ of the simulated CCF is equal (within 0.75 km s^{-1}) to the observed $\sigma_p^{\rm obs}$ value is recorded. The histogram of these numbers as a function of $\sigma_{\rm in}$ is akin to a probability distribution of the cluster velocity dispersion σ_p, given the magnitude of the integrated light $M_V^{\rm int}$ and the observed velocity dispersion $\sigma_p^{\rm obs}$. Fig. 12 gives nine examples of these $\sigma_{\rm in}$ probability distributions, for different pairs of input parameters $M_V^{\rm int}$ and $\sigma_p^{\rm obs}$. In these simulations, the absolute integrated-light magnitude $M_V^{\rm int} = -2, -4, -6$, correspond to numbers of added CCFs equal to N = 200, 1262, 8000, respectively.

The most striking features in these $\sigma_{\rm in}$ probability distributions are the wings towards the high $\sigma_{\rm in}$, values, observed only when $M_V^{\rm int}$ is fainter than about -4.5 (see Fig. 12). These tails represent the cases where, for a globular cluster with whatever

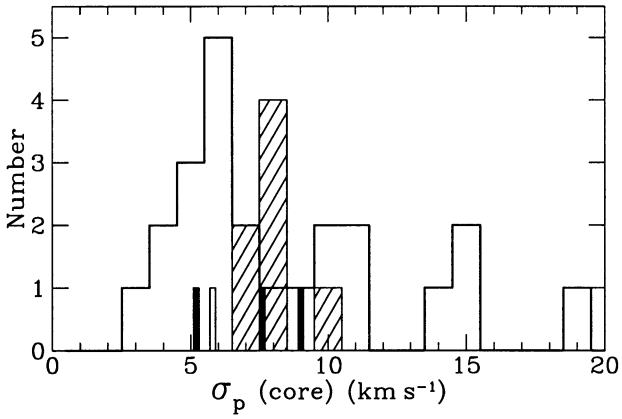

Fig. 10. Distributions of the core velocity-dispersion determinations of globular clusters belonging to the Galaxy (empty histogram), to the LMC (dashed histogram), to the SMC (one cluster displayed as an empty rectangle), and to the Fornax dwarf spheroidal galaxy (three clusters displayed as filled rectangles).

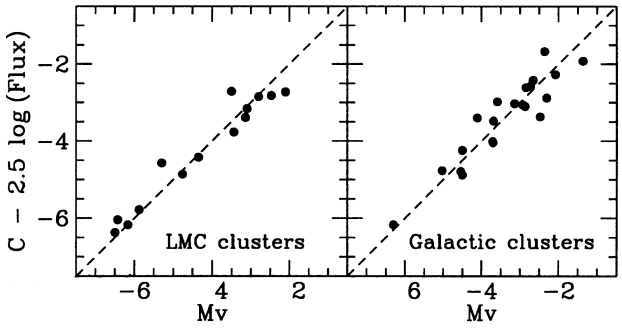

Fig. 11. Relation between $M_V^{\rm int}$ obtained from the mean flux in the continuum of the integrated-light spectra and $M_V^{\rm int}$ derived from the published central surface brightness values taken from Webbink (1985) and Mateo (1987).

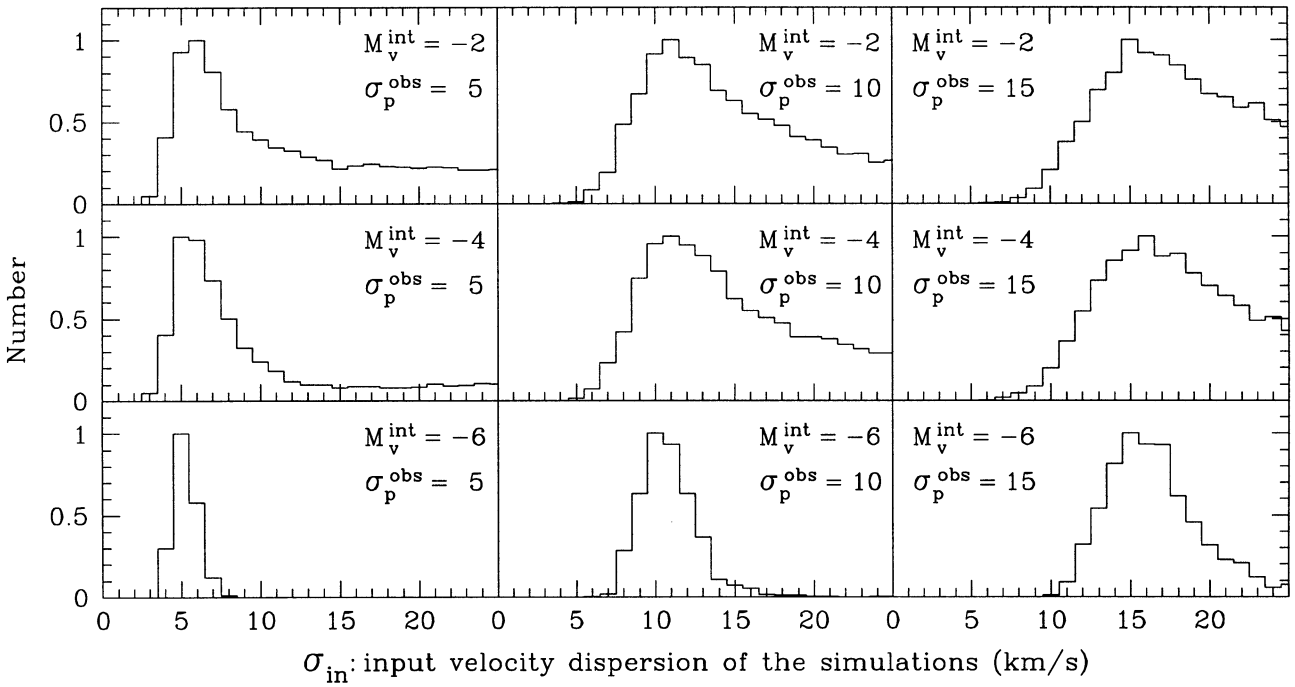

Fig. 12. Results of the numerical simulations. For any given absolute magnitude $M_V^{\rm int}$ of the integrated light in the aperture, different sets of 5000 simulated CCFs are computed for each $\sigma_{\rm in}$ value (from 1 to 26 km s^{-1} by step of 1 km s^{-1}). Each diagram shows the relative numbers of simulated CCFs which have a standard deviation in the range of $\sigma_p^{\rm obs} \pm 0.75$ km s^{-1}, as a function of $\sigma_{\rm in}$. These histograms do not differ significantly if the range ± 0.75 km s^{-1} is reduced to ± 0.25 km s^{-1}. Each of them is akin to a probability distribution of the cluster velocity dispersion σ_p, given the value of the observed velocity dispersion $\sigma_p^{\rm obs}$ and of $M_V^{\rm int}$.

genuine velocity dispersion, a small velocity dispersion $\sigma_p^{\rm obs}$ is measured, since the integrated light is dominated by a single bright star. In these cases, the integrated-light CCF is equal to the brightest star CCF, barely widened, in the wings, by the smaller contribution of the numerous fainter cluster stars.

Another feature is the similarities between the $\sigma_{\rm in}$ probability distributions in the upper two rows in Fig. 12, obtained with $M_V^{\rm int}$ ranging from -2 to -4 (N from 200 to 1262 added CCFs). The noticeable exception is the high $\sigma_{\rm in}$ tail, which decreases slowly with increasing N. These similarities are the consequences of the fact that the luminosity ratios of the few brightest stars, e.g., the ratio of the brightest star to the second or third brightest star, do not depend strongly on the number N of stars. With larger N values, the brightest stars are on average brighter. This brightness ratio does not depend strongly on the luminosity, because of the constant slope (to first order) of the luminosity function. Nevertheless, with N larger than about 1262, i.e., $M_V^{\rm int}$ brighter than about -4, the $\sigma_{\rm in}$ probability distributions narrow regularly with increasing N, become more and more symmetric, and lose their high $\sigma_{\rm in}$ wing. This indicates that the probability to have one star dominating the light becomes much smaller with increasing N.

Instead of considering the probability distributions as a function of $\sigma_{\rm in}$ as in Fig. 12, it is possible to compute the probability distributions as a function $\sigma_{\rm in}/\sigma_p^{\rm obs}$, which do not depend much on the considered $\sigma_p^{\rm obs}$. Consequently, in first approximation, the $\sigma_{\rm in}/\sigma_p^{\rm obs}$ probability distributions are independent from the two simulation parameters $M_V^{\rm int}$ (or N) and $\sigma_p^{\rm obs}$, this within the $M_V^{\rm int}$ range from -2 to -4 in absolute magnitude. Within this magnitude range, the mode values of all probability distributions equal 1.08, and the lower and upper values at half of maximum equal 0.80 and 1,60. Consequently, the following expression can be used to deduce the best estimate of the cluster velocity dispersion σ_p:

$$\sigma_p \simeq \sigma_{\rm in} = (1.08^{+0.52}_{-0.28})\sigma_p^{\rm obs} \quad \text{if} \quad -4 \leq M_V^{\rm int} \leq -2\ . \tag{5}$$

When $M_V^{\rm int}$ is brighter than -4.5, numerical simulations are achieved with the $M_V^{\rm int}$ and $\sigma_p^{\rm obs}$ values of the considered cluster as input parameters of the simulations. In those cases, the resulting $\sigma_{\rm in}$ probability distributions are always symmetrical enough to allow a good Gaussian fit, which is used to derive the most probable σ_p and the statistical error due to the small sample of dominant stars.

Our estimates of the statistical error due to the small sample of dominant stars are given in column 10 of Tables 6 and 7 for each globular cluster from our sample. For globular clusters with $M_V^{\rm int}$ fainter than -4.5, the upper error limits are flagged by a colon, in order to remind (i) the presence of the high $\sigma_{\rm in}$ tail in the corresponding $\sigma_{\rm in}$ probability distribution and (ii) the fact that Eq. (5) is used to compute the statistical errors. Column 11 of these two tables displays, for each globular cluster, the most probable σ_pp and the total uncertainty which is the square root of the quadratic sum of both uncertainties given in column 9

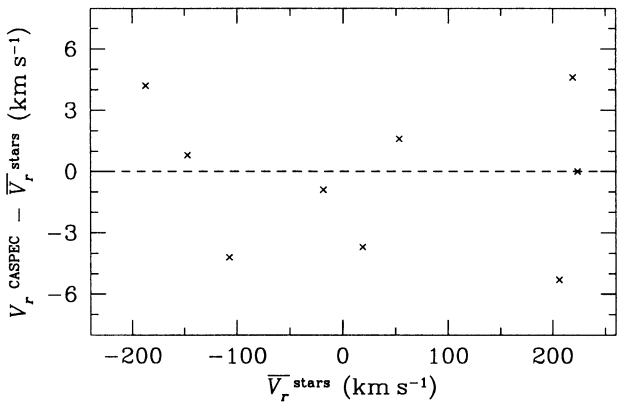

Fig. 13. For nine Galactic globular clusters, comparison of the radial velocities $V_r^{\rm caspec}$ derived in the present study from integrated-light spectra with the means $V_r^{\rm stars}$ from large numbers (> 40) of accurate radial velocities of cluster stars.

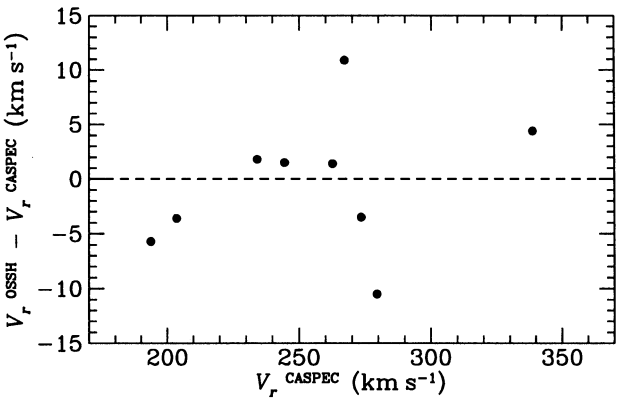

Fig. 14. For nine LMC old globular clusters, comparison of the radial velocities $V_r^{\rm caspec}$ derived in the present study from integrated-light spectra with the radial velocities $V_r^{\rm ossh}$ obtained by Olszewski et al. (1991).

and column 10. When a cluster is observed more than once, the $\sigma_p^{\rm obs}$ values have been averaged.

7. Comparison with previous V_r measurements

7.1. Galactic globular clusters

For nine Galactic globular clusters in our sample, accurate (≤ 1 km s^{-1}) radial velocities of at least 40 individual stars per cluster are given in the literature (see the compilation by Pryor & Meylan 1993). For each cluster, the average of these radial velocities gives an accurate ($\leq \pm 1$ km s^{-1}) cluster radial velocity $\overline{V}_r^{\rm stars}$. These radial velocities are compared, in Fig. 13, with the present radial velocities $V_r^{\rm caspec}$ derived from integrated-light spectra. The mean of the radial velocity differences $V_r^{\rm caspec}$ and $\overline{V}_r^{\rm stars}$, viz. -0.3 km s^{-1}, is not significantly different from zero. The standard deviation of these differences is 3.6 km s^{-1}. This value is larger than the 1.8 km s^{-1} expected from our error estimates given in column 3 of Table 6, but is perfectly consistent with our estimates of the statistical error due to small samples of dominant bright stars in determination of radial velocities from integrated-light spectra. Our numerical simulations described in Sect. 6 above, show that, for most galactic clusters, a statistical error of about 3 km s^{-1} affects our radial velocities. Consequently, the uncertainties of the radial velocities given in column 3 of Table 6 are probably underestimated, an uncertainty of about 3 km s^{-1} being a more realistic value.

7.2. Magellanic globular clusters

In Fig. 14, our radial velocities $V_r^{\rm caspec}$ for nine old LMC globular clusters are compared with the radial velocities $V_r^{\rm ossh}$ previously derived by Olszewski et al. (1991). Their velocities are the mean of the radial velocities of 2–4 giant stars per cluster. They derive the radial velocity of these individual giant stars, with an accuracy of 5 km s^{-1}, from measurement of the calcium triplet.

The mean of the radial velocity differences between $V_r^{\rm ossh}$ and $V_r^{\rm caspec}$ is -0.4 ± 2.1 km s^{-1}, again not significantly different from zero, and the standard deviation of these differences is 6.2 km s^{-1}. This agreement is remarkably good considering the small number of stars per cluster measured by Olszewski et al. (1991) – 2 stars in 6 of the 9 clusters – and the uncertainty of 5 km s^{-1} on their stellar radial velocities. Our numerical simulations (Sect. 6 above) show that the statistical error due to a small sample do not affect significantly our radial velocity determinations of the LMC globular clusters.

8. Comparison with previous σ_p measurements

8.1. Core velocity dispersion from V_r of individual stars

The estimates of the errors due to small number statistics derived in Sect. 6 are relatively large for many Galactic globular clusters (see Table 6). One way of checking the accuracy of our core velocity dispersion estimates consists of comparing our values with velocity dispersions computed from the radial velocity measurements of large numbers of individual stars. However, these velocity dispersions cannot be directly compared, since the individual stars measured are spread over areas much larger than the sampling areas of about $6'' \times 6''$ used for our integrated light spectra. In globular clusters, the projected velocity dispersion decreasing with increasing radius the velocity dispersions derived over large areas may be smaller than the core velocity dispersion. Nevertheless, the central velocity dispersion can be derived from radial velocities of individual stars by using dynamical models. This is done in a study by Pryor and Meylan (1993), who applied an isotropic multi-mass King model to available data from the literature for 56 Galactic globular clusters.

Radial velocities of individual stars are found in the literature for eight Galactic globular clusters from our sample (NGC 104, 362, 1904, 5272, 5904, 6681, 7078, and 7099). For these clusters, Fig. 15 displays the σ_0 from Table II of Pryor and Meylan (1993) as a function of the $\sigma_p^{\rm obs}$ and the σ_p derived in the

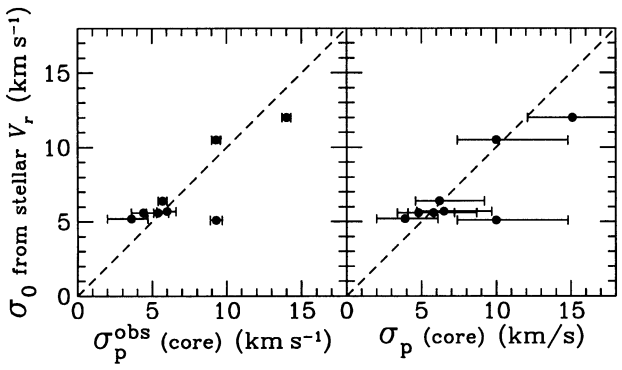

Fig. 15. For eight Galactic globular clusters, central velocity dispersions σ_0 (derived by Pryor & Meylan (1993) by fitting isotropic multi-mass King models to radial velocities of individual globular cluster stars), as a function of the velocity dispersion $\sigma_p^{\rm obs}$ (left panel) and σ_p (right panel), derived in the present study from integrated-light spectra.

present study, taken from column 9 and 11 of Table 6, respectively. Apart from the cluster NGC 6681, which lies below the dashed line, the agreement between σ_0 and $\sigma_p^{\rm obs}$ (or σ_p) is good. This suggests that our statistical error estimates – represented by the error bars in the right panel of Fig. 15 – are on average pessimistic. We show below several other pieces of evidence which suggest that the numerical simulations may overestimate the errors due to small number statistics.

8.2. Core velocity dispersion from integrated-light spectra

For nine Galactic globular clusters in our sample, velocity dispersions from integrated-light spectra are available from Illingworth (1976) and Zaggia et al. (1992). In Table 8 these velocity dispersions are compared with our results taken from column 9 and 11 of Table 6. In the three studies, the velocity dispersions are derived from different sampling areas. A 12″ to 24″ slit is used by Illingworth (1976), with no scanning on the cluster core during the exposure. The sampling areas used by Zaggia et al. (1992) are $5'' \times 4\farcs6$ in the case of NGC 5824 and $6'' \times 4\farcs6$ for their other 3 clusters. In our case, we use a sampling area of $5'' \times 5''$ for NGC 1851 and of $6'' \times 6''$ for the other 8 clusters. There are probably differences between the different studies – up to 3–4″ – on the positioning of the center of the sampling area on the cluster cores. Since these areas are not exactly the same in both size and positioning, it is unlikely that statistical errors due to small stellar samples affect similarly these different velocity dispersion determinations. The reasonably good agreement between the different results displayed in Table 8 is therefore another indication that our estimates of the statistical errors due to small samples are pessimistic.

Core velocity dispersions are also derived by Mateo et al. (1991) for several old LMC globular clusters. The uncertainties on their results are, however, much larger than ours.

Table 8. Core velocity dispersions from integrated-light spectra for Galactic globular clusters studied by different authors.

NGC	Illingworth (1976)	Zaggia et al. (1992)	Present study	
No.	σ_p(core) (km s^{-1})	σ_p(core) (km s^{-1})	σ_p^{obs} (km s^{-1})	σ_p(core) (km s^{-1})
104	10.5±0.4	...	$9.3^{+0.3}_{-0.3}$	$10.0^{+4.8}_{-2.6}$:
362	7.5±0.9	...	$5.7^{+0.3}_{-0.3}$	$6.2^{+3.0}_{-1.6}$:
1851	7.9±0.7	...	$10.5^{+0.4}_{-0.5}$	$11.3^{+2.5}_{-1.8}$
5824	...	12.8±0.5	$10.6^{+0.4}_{-0.4}$	$11.1^{+1.6}_{-1.6}$
6093	12.5±2.5	12.4±0.4	$13.4^{+0.6}_{-0.6}$	$14.5^{+7.0}_{-3.8}$:
6266	13.7±1.7	...	$14.3^{+0.4}_{-0.4}$	$15.4^{+7.4}_{-4.0}$:
6441	17.6±0.8	...	$18.1^{+0.2}_{-0.2}$	$19.5^{+9.4}_{-5.1}$:
6681	...	9.9±0.9	$9.3^{+0.4}_{-0.4}$	$10.0^{+4.8}_{-2.6}$:
7099	...	6.0±0.6	$5.3^{+0.5}_{-0.6}$	$5.8^{+2.9}_{-1.7}$:

9. Relation between velocity dispersion, luminosity, and a physical scale

Galactic globular clusters show tight correlations between velocity dispersion, luminosity and a physical scale. These correlations, which are analogous to the fundamental plane correlations for elliptical galaxies, have already been discussed by several authors (e.g., Meylan & Mayor 1986, Paturel & Garnier 1992, Djorgovski & Meylan 1994). Djorgovski (1995) shows that the scaling law, corresponding to the best fit to the currently available data for Galactic globular clusters, is consistent with the scaling law expected from the Virial Theorem. This suggests that globular clusters are virialized systems, with a universal and constant M/L ratio to within the measurement errors.

With a constant M/L ratio, the Virial Theorem predicts the following relation:

$$5 \log \sigma + 2.5 \log r_h = Cst - M_v \quad (6)$$

between the *global* velocity dispersion σ, the half-light radius r_h, and the absolute V magnitude M_V, whereas the King (1966) models lead to:

$$5 \log \sigma_0 + 2.5 \log \mu r_c = Cst - M_v \quad (7)$$

where σ_0 is the *central* velocity dispersion, μ the dimensionless mass, r_c the core radius, and M_V the absolute V magnitude. Figure 16 shows the relations between $5 \log \sigma + 2.5 \log r_h$ vs. M_v (first row), and $5 \log + 2.5 \log \mu r_c$ vs. M_v (second row), for different data sets. In panels a and b, we plot clusters with a *global* velocity dispersion measurement, based on radial velocities of individual stars, taken from the compilation of Pryor and Meylan (1993). In panels c, d, e, we plot clusters with a *core* velocity dispersion derived from integrated-light measurements in the present study. Half-light radii are taken from Trager et al. (1993), and cluster concentrations and core radii are from Pryor and Meylan (1993). In panels a and b, the continuous lines represent the relations (6) and (7), respectively, with best fitted constants. The dashed lines represent the relations obtained when

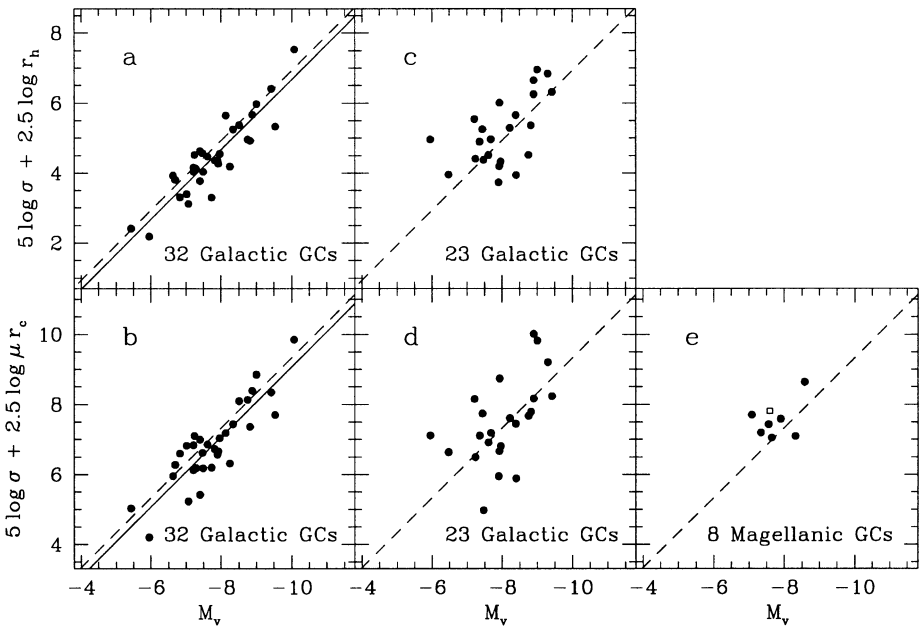

Fig. 16. Fundamental plane correlations for Galactic and Magellanic globular clusters: this figure shows a combination of the velocity dispersion σ_p with a physical scale (half-light radius r_h on the first row and the product of the dimensionless mass μ and the core radius r_c on the second) as a function of the absolute visual magnitude M_V. In panels a and b, we use the global velocity dispersions, based on radial velocities of individual stars. In panels c, d, e, we use the core velocity dispersions derived in the present study. The open square in panel e represents NGC 121, the only SMC cluster. The straight lines represent the relations derived from the Virial Theorem in panel a, and from the King models in panel b, using *global* (continuous lines) or *central* (dashed lines) velocity dispersions. The dashed lines in panels a and b are reproduced in panels c, d, and e, for the purpose of comparison.

central velocity dispersions (extrapolated for these clusters from King models by Pryor and Meylan 1993) are considered instead of the *global* velocity dispersion. For the purpose of comparison, the dotted line of panel a is drawn in panel c, and the dotted lide of panel b is reproduced in panels d and e.

In Fig. 16, when using *global* velocity dispersions based on radial velocities of individual stars, the standard deviations around the relation expected from the Virial Theorem is ~ 0.49 (panel a), while the standard deviations around the relation expected from the King models is ~ 0.65 (panel b). These standard deviations are comparable to the observational uncertainties (Pryor & Meylan 1993): the data do not show significant deviations from the Virial Theorem or the King models. Note that in panel b, it would be more appropriate to use central velocity dispersions instead of global ones.

When using *core* velocity dispersions from integrated-light measurements, the dispersions are somewhat larger in panels c and d (Galactic clusters). The standard deviation in panel c is 0.84, while the corresponding value is 0.49 in panel a. This increase is probably due, in part, to the larger uncertainties of the velocity dispersions derived from integrated light, and also to a possibly larger intrinsic scatter since this panel displays *core* velocity dispersions of high-concentration (collapsed?) globular clusters. A similar degradation is observed from panel b to panel d. Part of the scatter in panel d is probably due to the observational difficulties of measuring the very small core radius of the very high-concentration clusters.

The scatter observed in panel e for Magellanic clusters is similar to the scatter observed for Galactic clusters with velocity dispersions based on radial velocities of individual stars. This shows that our measurements for Magellanic clusters are reliable, and that their M/L ratios may be similar to the M/L ratios of Galactic clusters.

It is worth noticing that our simulations (see Sect. 6) show that statistical errors due to small samples lead, on average, to underestimates of the velocity dispersion. Therefore, if these errors were completely dominant, the Galactic clusters should lie below the expected relations in panels c and d. This is not observed, which, again, suggests that our statistical error estimates from Sect. 6 are somewhat pessimistic.

10. Discussion and conclusion

We present, in this paper, the radial velocity and velocity dispersion measurements deduced from integrated-light spectra obtained with CASPEC at the ESO 3.6-m telescope at La Silla, Chile, for a large sample of Galactic and Magellanic globular clusters. These measurements can be affected by large statistical uncertainties if the integrated light through the spectrograph slit is dominated by a small number of bright stars. We present a very extensive set of numerical simulations, which indicates that statistical uncertainties on the velocity dispersion values are small, i.e., comparable or smaller than the measurement uncertainty, when the absolute magnitude of the integrated light within the

measurement sampling area is brighter than an absolute V magnitude of about -4.5 (see Fig. 12). This result suggests that statistical uncertainties on our (and any other) velocity dispersion estimates are important for most Galactic clusters, and small in the case of Magellanic clusters.

However, the three following facts suggest that our simulation results may be somewhat pessimistic. First, there is a reasonably good agreement between our integrated-light σ_p measurements and the σ_p measurements based on radial velocities of individual stars found in the literature. Second, our results agree well with previous independent integrated-light up measurements, achieved over different sampling areas. Third, *on average*, our σ_p values are consistent with those expected from King models, given the cluster total absolute magnitude and structural parameters, as is the case for the σ_p values derived from the radial velocities of individual stars. This last point rules out the possible presence of a large bias in our measurements of Galactic clusters resulting from the light in our sampling area coming predominantly from a few bright giants.

In short, our simulations provide upper limits for the uncertainties due to the domination of too small a number of bright stars on the σ_p values. Consequently, when using our σ_p measurements one should keep in mind that the quoted statistical uncertainties may be overestimated. Because of the larger distances to the Magellanic globular clusters, all but one of the σ_p measurements obtained for the Magellanic clusters are fully reliable, with relatively small uncertainties, which nevertheless could also be overestimated.

We shall present, in a following paper (Dubath et al. 1996), a determination of the structural parameters for the Magellanic clusters, together with their M/L_V estimates based on the present σ_p measurements.

No significant deviation from the predictions of the King models, or from the Virial theorem, are observed in the globular cluster fundamental plane, as already discussed by several authors (e.g., Pryor & Meylan 1993) in the case of Galactic clusters. This shows that the globular cluster M/L_V is, within the accuracy of the data, constant from cluster to cluster, and that Magellanic clusters do not have a M/L_V dramatically different from those of Galactic clusters. As a consequence, the fundamental plane correlations can also be used to test our σ_p results. For example, the remarkably small scatter of the Magellanic cluster data around the relation expected from King models observed in Fig. 16 is another indication of the good quality of our σ_p measurements for these clusters.

The results of the simulations can also be used to predict the accuracy of any σ_p measurement from integrated-light observation. In order to get a reliable measurement, the absolute V magnitude of the integrated light should be brighter than -4.5. For a cluster of known brightness profile, this can be translated into a minimum aperture (i.e., a minimum number of stars) needed to get a meaningful σ_p measurement.

Acknowledgements. It is a pleasure to thank Tad Pryor, the referee, for his careful reading of the paper and his excellent suggestions for improvements. P.D. acknowledges support through a grant from the Swiss National Science Foundation.

References

Baranne A., Mayor M., Poncet J.L., 1979, Vistas Astron., 23, 279
Buonanno R., Buzzoni A., Corsi C.E., Fusi Pecci F., Sandage A.R., 1988, in IAU Symp. 126, The Harlow Shapley Symposium on Globular Cluster Systems in Galaxies, eds J.E. Grindlay & A.G. Davis Phillip (Dordrecht: Reidel), p. 621
Djorgovski S., 1995, ApJL, 438, 29
Djorgovski S.,Meylan G., 1994, AJ, 108, 1292
Dubath P., Meylan C., 1994, A&A, 290, 104
Dubath P., Meylan G., Mayor M., 1990, A&A, 239, 142
Dubath P., Meylan G., Mayor M., 1992, ApJ, 400, 510
Dubath P., Meylan G., Mayor M., 1994, ApJ, 426, 192
Grabhorn R.P., Cohn H.N., Lugger P.M., Murphy B.W., 1992, ApJ, 392, 86
Griffin R.F., 1968, A Photometric Atlas of the Spectrum of Arcturus, Cambridge, Phil. Soc.
Guhathakurta P., Yanny B., Schneider D., Bahcall J.N., 1996, AJ, 111, 267
Hesser J.E., Hartwick F.D.A., 1977, ApJS, 33, 361
Hesser J.E., Harris W.E., VandenBerg D.A., et al., 1987, PASP, 99, 739
Illingworth G., 1976, ApJ, 204, 73
King, I.R. 1966, AJ, 71, 64
King I.R., Piotto C., Cool A.M., Anderson J., Sosin C., 1996, in the ESO/STScI workshop on Science with the Hubble Space Telescope – 11, eds. Benvenuti P., Macchetto F.D. & Schreier E.J. (Baltimore: STScI), in press
Mateo M., 1987, ApJ, 323, L41
Mateo M., Welch D., Fischer P., 1991, in IAU Symp. 148, The Magellanic Clouds, eds R. Haynes & D. Milne (Dordrecht: Kluwer), p. 191
Mayor M., Maurice E., 1985, in: Stellar Radial Velocities, eds A.G. Davis Philip & D.W. Latham (L Davis Press), p. 299
Meylan G., Dubath P., Mayor M., 1991, ApJ, 383, 587
Meylan G., Mayor M., 1986, A&A, 166, 122
Meylan G., Mayor M., Duquennoy A., Dubath P., 1995, A&A, 303, 761
Norris J., Bessel M.S., Pickles A.J., 1985, ApJS, 58, 463
Olszewski E.W., Schommer R.A., Suntzeff N.B., Harris H.C., 1991, ApJ, 101, 515
Paturel G., Gamier R., 1992, A&A, 254, 93
Peterson R.C., Seitzer P., Cudworth K.M., 1989, ApJ, 347, 251
Pryor C., Meylan G., 1993, in Structure and Dynamics of Globular Clusters, ASP Conference Series, Vol. 50, eds S. Djorgovski & G. Meylan (San Francisco: ASP), p. 357
Reijns R., Le Poole R., De Zeeuw T., Seitzer P., Freeman K., 1993, in Structure and Dynamics of Globular Clusters, ASP Conference Series, Vol. 50, eds S. Djorgovski & G. Meylan (San Francisco: ASP), p. 79
Sosin C., King I.R., 1996, in Dynamical Evolution of Star Clusters: Confrontation of Theory and Observations, IAU Symp. 174, eds. Hut P. & Makino J. (Dordrecht: Kluwer), in press
Trager, S.C., Djorgovski, S., King, I.R., 1993, in Structure and Dynamics of Globular Clusters, ASP Conference Series, Vol. 50, eds S. Djorgovski & G. Meylan (San Francisco: ASP), p. 347
Webbink R.F., 1985, in IAU Symp. 113, Dynamics of Star Clusters, eds J. Goodman & P. Hut (Dordrecht: Reidel), p. 541
Zaggia S., Capaccioli M., Piotto C., Stiavelli M., 1992, A&A 258, 302
Zaggia S., Capaccioli M., Piotto G., 1993, A&A, 278, 415